Technical Report

TR-08-07

Assessment of the radium-barium co-precipitation and its potential influence on the solubility of Ra in the near-field

Fidel Grandia, Joan Merino, Jordi Bruno
Amphos[21]

Augusti 2008

Svensk Kärnbränslehantering AB
Swedish Nuclear Fuel
and Waste Management Co
Box 250, SE-101 24 Stockholm
Tel +46 8 459 84 00

Assessment of the radium-barium co-precipitation and its potential influence on the solubility of Ra in the near-field

Fidel Grandia, Joan Merino, Jordi Bruno
Amphos[21]

Augusti 2008

Summary

Radium 226 is one of the main contributors to radiological dose in some of the scenarios contemplated in the recent SR Can safety assessment. /SKB 2006a/. The relative contribution of the ^{226}Ra dose is clearly dependent on the source term value for this radionuclide, which is directly connected to its solubility behaviour. Most of the source term calculations performed for this radionuclide pessimistically assume that its solubility is controlled by the individual solubility of $RaSO_4(s)$, the most insoluble phase under near field conditions, while the abundant information from early radiochemical research, natural system studies and anthropogenic systems would indicate that Ra(II) is mainly associated to $BaSO_4(s)$ precipitation.

In this work we have investigated the extensive literature concerning the mechanisms and processes controlling the co-precipitation/solid solution formation behaviour of the Ra(II)/Ba(II) sulphate system. We have also established the necessary thermodynamic moles to model the solubility behaviour in the vicinity of the spent fuel system.

Calculations using an ATM-104 fuel at 40 MWd/kg U show that barium and radium inventories per canister progressively grow with time after deposition, most of the barium is produced in the initial 500 years. In the unlikely event of a contact of sulphate-containing groundwaters with the fuel, Ba(II) will precipitate as $BaSO_4(s)$. The production of ^{226}Ra reaches its peak some 300,000 years after deposition. This substantial time gap indicates that most of the $BaSO_4(s)$ will be present when and if radium is released from the fuel, even if some Ra(II) and Ba(II) will be released contemporaneously.

Two potential scenarios have been addressed from the mechanistic point of view. In the event of a simultaneous release of Ra with Ba, the former will be readily incorporated into the precipitating $BaSO_4$ to build a Ra Ba sulphate solid solution. All the existing evidence indicates, that in this case, the behaviour of the system can be described by the established aqueous-solid solution thermodynamic formalism and assuming that the system behaves ideally. In the case when ^{226}Ra is released from a secondary source, like a UO_2 precipitate away from the fuel but within the canister, there is not sufficient experimental information at the molecular level to establish when and how the system will reach equilibrium and, therefore, it is not clear to which extent the aqueous-solid solution thermodynamic formalism can be applied. Nevertheless, the long contact times expected under repository conditions together with the small mass transfer processes involved would indicate that it is quite likely that equilibrium will be reached. Dedicated experimental investigations are under way in collaboration with INE-KFZ to establish the mechanism and rates of this critical process in order to support the solid solution thermodynamic approximation.

We have performed a number of scoping calculations in order to establish the absolute and relative effects of $RaBaSO_4(ss)$ formation on ^{226}Ra solubility. We have assumed that the free volume per canister filled by water in case of intrusion is roughly 1 m^3. By using the standard fuel dissolution rate of 1.0×10^{-7} y^{-1}, and a congruent release of barium, the calculated radium and barium concentrations after one year of contact at the disposal time of 300,000 years (when the ^{226}Ra content is largest), are 1.3×10^{-12} and 4.9×10^{-9} $mol\cdot L^{-1}$, respectively. If we apply the thermodynamics of aqueous-solid solution equilibria the resulting solid phase in equilibrium has a calculated nominal composition of $(Ba_{0.99942}Ra_{0.00057})SO_4$ (ss) and the resulting dissolved Ra(II) is in the 10^{-11} mol L^{-1} range. This is in the upper range of any observed Ra(II) concentration in natural and anthropogenic environment. If the solubility of Ra(II) is assumed to be controlled by the precipitation of a pure sulphate phase, the resulting concentration is three orders of magnitude higher. A concentration never observed in natural systems.

Since sulphate concentration can be highly variable due to changes in the nature of the groundwaters flowing into the near field, we have performed a sensitivity study of the influence of the sulphate concentrations in the expected concentration range. In the case when the lowest concentration is assumed ($[SO_4^{2-}] = 3\times10^{-4}$ $mol\cdot L^{-1}$), the calculated radium solubility increases up to 7.1×10^{-10} $mol\cdot L^{-1}$ when equilibrium with the solid solution is considered.

Sammanfattning

Radium-226 är en av de radionucklider som ger det största bidraget till den beräknade dosen i några av de scenarier som presenterades i säkerhetsanalysen SR-Can /SKB 2006a/. Det relativa bidraget av dosen från ^{226}Ra är beroende på värdet på källtermen för denna nuklid, vilket i sin tur är beroende på dess löslighet. De flesta källtermsberäkningar som genomförts för denna nuklid har pessimistiskt antagit att lösligheten är bestämd av den individuella lösligheten hos $RaSO_4(s)$, vilken är den mest svårlösliga fasen under de förhållanden som råder i förvarets närområde. Det finns dock omfattande information från tidig radiokemisk forskning samt studier av naturliga och antropogena system som indikerar att Ra(II) i huvudsak är associerad med fällningar av $BaSO_4$.

I den här studien har vi genomfört en omfattande litteraturstudie av de mekanismer och processer som kontrollerar medfällnings/fast lösningsbeteendet hos Ba(II)/Ra(II)-sulfatsystemet. Vi har också tagit fram den termodynamiska modell som behövs för att kunna beskriva lösligheten beteende i närheten av det använda bränslet.

Beräkningar baserade på ett ATM-104 bränsle med en utbränning av 40 MWd/kgU visar att inventarierna av barium och radium ökar med tiden efter deponering. Det mesta bariumet produceras de första 500 åren. I det osannolika fallet där grundvatten kommer i kontakt med bränslet, kommer Ba(II) att falla ut som $BaSO_4(s)$. Produktionen av ^{226}Ra når sin topp vid ungefär 300 000 år efter deponeringen. Denna tidsförskjutning indikerar att $BaSO_4(s)$ redan kommer att förekomma om och när radium frigörs från bränslet, även om en del Ra(II) och Ba(II) kommer att frigöras kongruent.

Två potentiella utvecklingar har behandlats från ett mekanistiskt synsätt. Om Ra och Ba frigörs simultant, kommer den förstnämnda att direkt inkorporeras i den bildade $BaSO_4$ och bilda en Ra-Ba-sulfat fast lösning. All existerande information visar att i det här fallet kan systemets beteende beskrivas med etablerade lösning-fast lösning termodynamiska formuleringar och det går att förutsätta att systemet uppför sig idealt. I fallet när ^{226}Ra frigörs från en sekundär källa, exempelvis en utfällning av UO_2 på avstånd från bränslet men fortfarande inuti kapseln, finns det inte tillräcklig experimentell information på molekylär nivå för att bedöma när och hur systemet når jämvikt och det är därför inte uppenbart hur en lösning-fast lösning termodynamisk formulering kan tillämpas. De långa kontakttiderna förväntade under förvarsförhållanden tillsammans med de mycket långsamma masstransportprocesserna indikerar dock att det är mycket troligt att en jämvikt kommer att nås. Särskilda experimentella studier är planerade tillsammans med INE-KFZ för att bestämma mekanismer och hastigheter för denna kritiska process för att ge stöd till användandet av en fast lösning termodynamisk approximation.

Vi har genomfört ett antal beräkningar för att bedöma den absoluta och relativa betydelsen av bildandet av en $RaBaSO_4(ss)$ för lösligheten för ^{226}Ra. Vi har antagit att den fria volymen inuti en vattenfylld kapsel är ungefär 1 m^3. Med antagandet om en bränsleupplösningshastighet av 1×10^{-7} y^{-1} och kongruent frigörelse av barium, beräknades koncentrationerna av radium och barium till $1{,}3\times10^{-12}$ mol·L-1 respektive $4{,}9\times10^{-9}$ $mol\cdot L^{-1}$ efter ett års kontakttid vid en genombrottstid vid 300 000 år (då radiumhalten är störst). Med termodynamisk jämvikt för lösning-fast lösning kommer den fasta fasen i jämvikt att ha en beräknad sammansättning av $(Ba_{0,99942}\ Ra_{0,00057})SO_4(ss)$ och den resulterande halten Ra(II) i lösning hamnar runt 10^{-11} $mol\cdot L^{-1}$. Detta överensstämmer med de maximala radiumhalter som har mätts i naturliga och antropogena system. Om lösligheten för Ra(II) antas vara kontrollerad av utfällningen av en ren sulfatfas kommer koncentrationen att vara tre storleksordningar högre. En sådan koncentration har aldrig observerats i naturliga system.

Eftersom sulfatkoncentration i grundvattnet i närområdet har en stor naturlig variabilitet, har vi genomfört en känslighetsstudie av sulfathalter i det förväntade intervallet för att bedöma betydelsen av detta. I fallet där den lägsta sulfathalten är antagen ($[SO_4^{2-}] = 3\times10^{-4}$ $mol\cdot L^{-1}$), ökar lösligheten för radium till $7{,}1\times10^{-10}$ $mol\cdot L^{-1}$ i jämvikt med den fasta lösningen.

Contents

1 Introduction

Radium 226 is one of the main contributors to radiological dose in some of the scenarios contemplated in the recent SR Can safety assessment. /SKB 2006a/. For instance, in the growing pinhole scenario the main dose contributors are ^{129}I and ^{226}Ra, the later becoming the dominant one after 50,000 years of repository lifetime. This dominance of the ^{226}Ra dose is clearly dependent on the source term value for this radionuclide, which is directly connected to its solubility behaviour. This has been illustrated in some of the sensitivity calculations performed in SR-Can where for the cases in which the Ra solubility limit was attained, the effect on the resulting dose was quite substantial (see for instance Figure 1-1, extracted from /SKB 2006a/).

The solubility behaviour of ^{226}Ra is quite uncertain depending on the process considered. Most of the source term calculations performed for this radionuclide pessimistically assume that its solubility is controlled by the individual solubility of $RaSO_4(s)$, the most insoluble phase under near field conditions, while the abundant information from early radiochemical research, natural system studies and anthropogenic systems would indicate that Ra(II) is mainly associated to $BaSO_4(s)$ precipitation. The affinity of the radium ion with the barite crystal lattice comes from the similarity of barium and radium ionic radius (1.36 Å and 1.43 Å, respectively), so that it is expected to be well accommodated in this structure. In addition, the fact that the polarizability of both ions is almost identical (see Table 1-1) indicates a clear preference for Ra^{2+} to substitute for Ba^{2+} in the ionic crystal lattice of Ba(II) sulphate /Goldschmidt 1938/.

This similarity in polarizability lies behind the fact that $(Ba,Ra)SO_4$ solid solutions are thermodynamically more stable than the simple mechanical mixture between solid solution end-members ($BaSO_4$ and $RaSO_4(s)$) even at trace concentrations of one of them. The reason for this higher stability is found in the reduction of the Gibbs free energy when a solid solution forms (see a thorough discussion of this in Chapter 2 of /Bruno et al. 2007/). Consequently, radium will preferentially be incorporated into barite, lowering the aqueous radium concentrations in equilibrium.

Table 1-1. Polarizability of selected divalent cations (Å³) /Goldschmidt 1938/.

Be^{2+}	Mg^{2+}	Ca^{2+}	Sr^{2+}	Ba^{2+}	Ra^{2+}
5.6	10.6	22.8	27.6	39.7	38.3

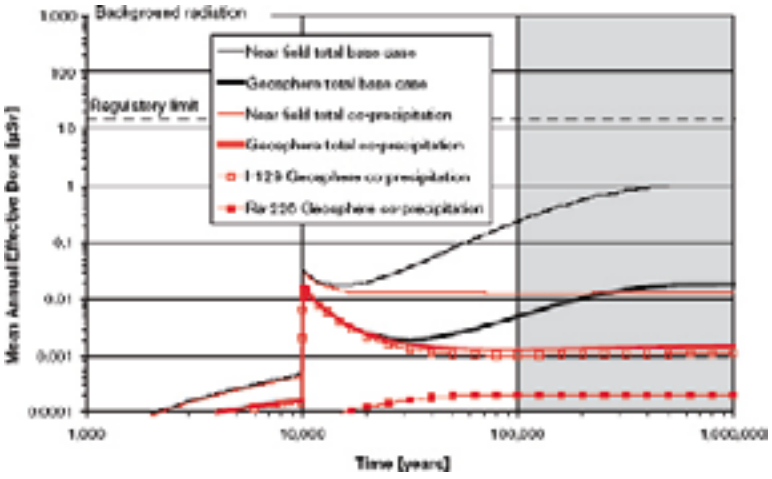

Figure 1-1. *Illustration of possible effect of co-precipitation of radium on the mean annual effective dose as calculated in the Forsmark pinhole failure base case (from /SKB 2006a/).*

In order to discuss the potential scenarios for Ra(II) behaviour in the vicinity of the spent fuel it is necessary to remind ourselves about the main processes that control the transfer of radionuclides from aqueous to solid solutions.

From the process perspective, we describe the transfer and distribution of chemical components between an aqueous and an adjacent solid phase under the general term of **sorption**.

Mechanistically sorption may occur through different mechanisms but the main ones are:

Adsorption: the accumulation of the chemical component at the interface without the development of a three dimensional molecular arrangement.

Absorption: the uptake by diffusion of the aqueous chemical component into the entire volume of an existing porous solid.

Precipitation: the transfer of a chemical component from an aqueous to a solid phase building a three dimensional molecular arrangement, e.g. the formation of $RaSO_4(s)$.

Coprecipitation: the precipitation and crystal growth process in which the minor component (Ra^{2+}) forms a common (mixed-composition, for instance $Ra_xBa_{1-x}SO_4(s)$) structure with the major component: $BaSO_4(s)$. This will certainly require the oversaturation with respect to the major component while the minor component $RaSO_4(s)$ is undersaturated.

Recrystallisation: the process of crystal rebuilding of the solid in contact with the aqueous solution. In the case of mixed solid phases this can be the main driving force for the formation of solid solutions at low temperature. In our case this would be the relevant process for the formation of a $(Ra,Ba)SO_4$ solid solution at the prevailing low temperatures expected in the near field after a few thousand years.

Solid solution: the homogeneous crystalline solid in which one or more atomic constituents are partially substituted without changing the original structure, although with some variation of the lattice parameters.

In this context, adsorption, surface precipitation and coprecipitation are precursory mechanisms for the formation of solid solutions, although regular molecular arrangements would require additional reorganisation mechanisms like ion-diffusion into the bulk of the solid and/or recrystallisation of the initial solid phase.

The formation of $(Ba,Ra)SO_4$ solid solutions seems to be a feasible mechanism since both Ba and Ra are produced in the spent fuel from the decay of several radioisotopes. In addition, a sizeable amount of barium (^{138}Ba) is already present in the spent fuel as a fission product. Each canister will contain about 6.6 kg of barium after 100,000 years of spent fuel disposal. Barite solubility is very low ($K_{ps} = 10^{-9.97}$) so that trace to minor amounts of barium in solution are sufficient to precipitate barium sulphate.

There are two main potential scenarios for Ra(II), Ba(II), sulphate coprecipitation in the vicinity of the spent fuel which we will discuss separately:

1. The **coprecipitation** of primary ^{226}Ra generated and released contemporaneously with ^{139}Ba from spent fuel and the sulphate present in the vicinity of the fuel.
2. The **surface precipitation** on existing $BaSO_4(s)$ of secondary ^{226}Ra generated from a uranium(IV) dioxide phase produced as a result of the initial release of U(VI) from the spent fuel surface and a later precipitation of the U(IV) dioxide as a consequence of the prevailing H_2/Fe reducing conditions in the interior of the canister. This initial surface precipitate would evolve towards a Ra(II), Ba(II) sulphate solid solution by **recrystallisation** and/or Ra^{2+} **diffusion** into the $BaSO_4(s)$ lattice.

These mechanisms and their consequences are rather different and will deserve a differentiated discussion in coming sections of this report.

In either case, the solubility of Ba(II) sulphate and, therefore, the potential formation of a solid solution will depend on the availability of sulphate in the near field. Sulphate concentrations in bentonite porewaters close to the canister are affected by processes such as:

1. The equilibration of the bentonite porewater with sulphate minerals, mainly gypsum, anhydrite and celestite. This reaction is strongly affected by the thermal field caused by canister heating /Arcos et al. 2006/.
2. Changes in the chemistry of groundwater flowing into the near field. Climatic changes, especially those related to glacial cycles, are able to substantially modify the composition of groundwater entering the near field.

In glacial stages, dilute waters will infiltrate down and changing the porewater composition.

The time and extent of $(Ba,Ra)SO_4$ solid solution precipitation is difficult to predict since it depends on the coupled effect of primary or secondary ^{226}Ra production and the sulphate concentration of the contacting fluid. In order to establish the time windows for potential solid solution formation in the vicinity of the spent fuel we need to calculate the evolution of ^{226}Ra, Ba and sulphate concentrations with repository time. This will be done in Section 3.

1.1 Objectives

The overall objective of this report is to establish the mechanistic and thermodynamic conditions under which it would be plausible to use $RaBaSO_4$ solid solution formation as a solubility control for ^{226}Ra.

In order to do this we will fulfil the following subsidiary objectives:

1. We will review and document the abundant radiochemical and geochemical information concerning the Ra(II), Ba(II), sulphate solid solution-aqueous system.
2. From the literature review we will establish the extent to which the kinetics and thermodynamics of this process are sufficiently known to document and calculate the effects of the coprecipitation scenarios discussed in the previous section.
3. Finally, we will calculate the conditions under which the $RaBaSO_4$ solid solution formation could control the solubility of ^{226}Ra in the vicinity of the fuel.

2 Review of the state-of-the-art of (Ba,Ra)SO_4 co-precipitation

2.1 The radiochemistry of ^{226}Ra and its relation to Ba(II) sulphate co-precipitation

The discovery of the element radium by Marie Curie and the subsequent investigations in the early days of Radiochemistry were very much connected to its coprecipitation with barium sulphate. The affinity of radium to barium sulphate was first reported by Marie Curie in her radium discovery work /Curie et al. 1898/. Later, in her Nobel Prize lecture /Curie 1911/, she detailed that she used barite extracts of the uranium residues in the St. Joachimsthal uranium mine (Czech Republic) for the recovery of the radium.

Radium uptake on barium sulphate was later reported by /Germann 1921/, who observed in his experiments that a certain quantity of radium from a solution of radium-barium chloride was *lost* when barium sulphate was added. He considered the uptake mechanism as $RaCl_2$ adsorption onto barite surface, and he modelled this process by applying the Freundlich adsorption isotherm.

The formation of (Ba,Ra)SO_4 solid solutions was thoroughly studied by /Doerner and Hoskins 1925/. From their recrystallisation and coprecipitation experiments they introduced the following distribution law (Equation 2-1):

$$\frac{\{Ra\}_{surface}}{\{Ba\}_{surface}} = \lambda \frac{[Ra]_{solution}}{[Ba]_{solution}} \qquad \text{(Equation 2-1)}$$

where $\{Ra\}_{surface}$ and $\{Ba\}_{surface}$ are the element fraction on the solid surface, $[Ra]_{solution}$ and $[Ba]_{solution}$ are the total Ra(II) and Ba(II) concentrations in solution, and λ is a proportionality constant (also called *heterogeneous partition coefficient*).

This empirical distribution law would later be known as the *Doerner-Hoskins distribution law*. It has been used extensively to describe element partitioning between aqueous and solid solution phases in many natural and laboratory systems. It has to be pointed out, though, that this distribution law does not take into consideration either the aqueous speciation of the components involved or the activities of the solids formed and, therefore, has limited thermodynamic value. Furthermore, the analysis of distribution coefficients obtained in different experiments would have to take into consideration their experimental conditions in order to make meaningful comparisons.

From Equation 2-1, /Doerner and Hoskins 1925/ concluded that *some radium will precipitate no matter how small its concentration*. They calculated the λ value for their experiments to be 1.8.

/Marques 1936/ carried out experiments similar to those of /Doerner and Hoskins 1925/ and she found similar λ (between 1.6 and 1.7). Later, /Gordon and Rowley 1957/ performed quite extensive coprecipitation experiments following the *homogeneous solution* technique at variable temperature (50 to 90°C). At 90°C, they found that the heterogeneous partition coefficient was dependent on the fraction of barium precipitated according Equation 2-2:

$$\lambda = 1.21 + 0.009 f \qquad \text{(Equation 2-2)}$$

where f is the fraction of barium precipitated. This resulted in a rather constant value for λ over a wide range of f. From experiments at 50 and 70°C, they were able to deduce a T-dependent function for λ (Equation 2-3):

$$\log_{10} \lambda = \frac{220}{273 + t} - 0.520 \qquad \text{(Equation 2-3)}$$

so that at higher temperatures λ was smaller.

After all these experiments, radium coprecipitation with barite has been reported in numerous studies in a range of scientific disciplines in both natural and laboratory environments. We will discuss the main results in Section 2.3.

2.2 Introduction to the barite isostructural group

The geochemistry of the barite isostructural group has been thoroughly studied. Solid solutions in this group may have contributions from four sulphate end-members, which are barite ($BaSO_4$), celestite ($SrSO_4$), anglesite ($PbSO_4$), and $RaSO_{4\,(c)}$. Aside from these solids, hashemite ($BaCrO_4$) and olsacherite ($Pb_2(SO_4)(SeO_4)$) also share a barite-type structure /Hawthorne et al. 2000/. However, barite and celestite are the only ones commonly found in natural environments. Anglesite is common in alteration zones in lead ore deposits. Radium sulphate has not been observed outside the laboratory. In synthetic Ba(II) sulphate samples, anionic substitution of sulphate by MnO_4^{2+} and SeO_4^{2+} has also been reported /Chang et al. 1996/.

The more common solid solution within this group is $(Ba,Sr)SO_4$, and, therefore many studies have been directed to investigate this solid solution system (e.g. /Felmy et al. 1993, Glynn 2000, Prieto et al. 2000, Pina et al. 2004, YuHang et al. 2007/). A recent review has been made by /Hanor 2000/. This binary solid solution system was initially treated as ideal (see Appendix A for solid solution concepts), and a complete solid solution series could be obtained at room temperature /Grahmann 1920/. However, the detailed analysis of natural samples showed a bimodal distribution, in which the Ba-rich and Sr-rich end members predominate. These are barite containing commonly less than 7 mol% $SrSO_4$ and celestite less than 4 mol% $BaSO_4$; /Hanor 1968/. Coprecipitation experiments of $(Ba,Sr)SO_4$ /Goldschmidt 1938, Starke 1964, Church 1970/ gave empirical partition coefficients of Sr in $BaSO_4$(s) (D_{Sr-Ba}) that ranged between $10^{-1.5}$ and 10^{-4} at room temperature. This would indicate that while Ba(II) is largely in the solid phase, Sr(II) mainly remains in solution. These observations would be in agreement with the calculations made by /Prieto et al. 1997/, who suggested that the precipitation of Sr(II)-rich solid solutions was only possible from aqueous solutions with a very low content on Ba(II) and that a wide range of solid solutions ($0.1 < BaSO_4\ x < 0.9$) were in equilibrium with a narrow range of aqueous solutions ($0.00005 < Ba,\ aq\ x < 0.004$). This behaviour in the $(Ba,Sr)SO_4$ system is interpreted to be caused by the large difference in the solubility products (three orders of magnitude) of the end members, and in the existence of a miscibility gap, which could also be rationalised in terms of the different polarizability of Sr^{2+} as compared to Ba^{2+} and Ra^{2+} (see Table 1-1).

The scientific interest in $(Ba,Pb)SO_4$ binary solid solution (hokutolite) arose from the evidence that this system may control the mobility of radium(II) during uranium ore processing /Kornicker et al. 1991/. In fact, radium incorporation into hokutolite has been observed in geothermal systems (e.g. /Momoshima et al. 1997/, and references therein). Complete $(Ba,Pb)SO_4$ solid solutions were synthesized in the laboratory /Boström et al. 1967, Wang et al. 2002, Lee et al. 2005/, although most of them were only metastable within a miscibility gap between 25 and 75% $PbSO_4$ /Takano et al. 1969/. In some studies, this solid solution has been treated as non-ideal (e.g. /Glynn 1990/).

/Zhu 2004a/ has recently reviewed the binary mixing properties of solid solutions in the barite isostructural family ($BaSO_4$, $SrSO_4$, $PbSO_4$, $RaSO_4$ and $BaCrO_4$). He calculated the parameters of non-ideality (interaction parameters, see Appendix A), partitioning coefficients and miscibility gaps for each binary solid solution in the system. From these data, he could confirm that elements with end-member solubility product lower than their host mineral phase are partitioned into the solid and depleted in the aqueous phase. Therefore, Ra^{2+} is expected to be readily incorporated into the barite lattice, as it is commonly observed.

The synergic effect of the presence of Sr(II) on the coprecipitation of Ra(II) with $BaSO_4$(s) was studied by /Goldschmidt 1938/. His investigations brought evidence of the synergistic role of Sr(II) in the Ra/Ba distribution in sulphate precipitates rendering very difficult the fractionation of Ra(II) in the presence of Ba(II) and Sr(II) sulphate, which was the original objective of his research. The following Figure 2-1 is extracted from Goldschmidt's work /Goldschmidt 1938/ and is a plot of the distribution coefficient of Ra(II) in the sulphate solid as a function of the Sr/Ba ratio in solution. It is noticeable that the partition is enhanced as a function of the Sr(II)/Ba(II) ratio in the aqueous phase. This would indicate that the presence of Sr(II) has a synergic effect rather than a competitive one with $BaSO_4$. This has interesting implications for the system under study in this report.

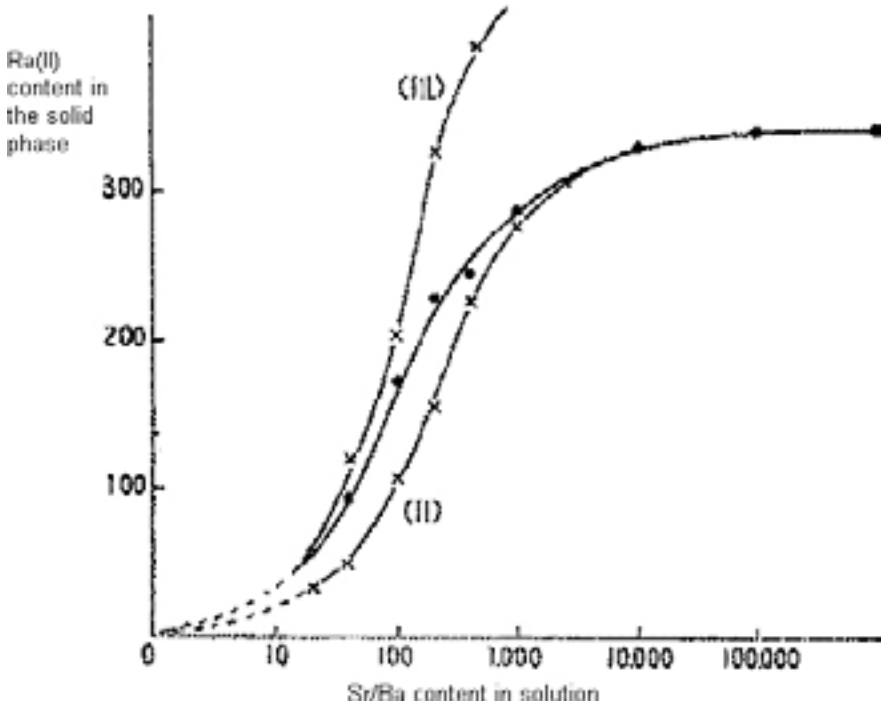

Figure 2-1. *Plot of the partition coefficient of Ra(II) in the total solid sulphate mass as a function of the Sr(II) to Ba(II) ratio in solution. The uptake of Ra(II) is enhanced at larger Sr(II)/Ba(II) ratios. From /Goldschmidt 1938/.*

2.3 Radium occurrences in surface and groundwaters and the role of barite on the Ra(II) solubility limit

The continuous monitoring of radium concentration in surface and ground waters has long been included in the water quality programs of environmental agencies due to the potential health risk of this element. In most instances, radium concentrations in natural environments are low ($< 10^{-11}$ mol·L^{-1}; Figure 2-2). This is mainly the result of the low radium content in common rocks and/or the active retention processes of this element. A common feature in most of the analysed waters is that the solubility limit of the least soluble individual solid ($RaSO_4$(s), log K_{ps}(25°C) = –10.26) is never reached, even in samples in which [Ra(II)] is anomalously high. In most cases radium-barium sulphate coprecipitation is proposed as the mechanism responsible for this behaviour (e.g. /Beaucaire et al. 1987, Sturchio et al. 1993, Grundl and Cape 2006/). The formation of (Ba,Ra)SO_4 solid solutions in natural environments has long been known, specially in geothermal areas, where barite was early recognized to be *radioactive* (e.g. /Knett 1904/). In Figure 2-2, barium and radium contents in waters from different origins are compared. In many cases a Ba-Ra positive correlation is evidenced. A potential exception could be found in the data for brines from the Palo Duro basin (USA), /Langmuir and Melchior 1985/. However, the extremely low measured Ra(II) concentrations together with the small range of variability of the Ra/Ba ratios would hamper any further analysis. In addition, the apparent divergence from the correlations found in other environments could be the result of the ionic strength effects in the brines.

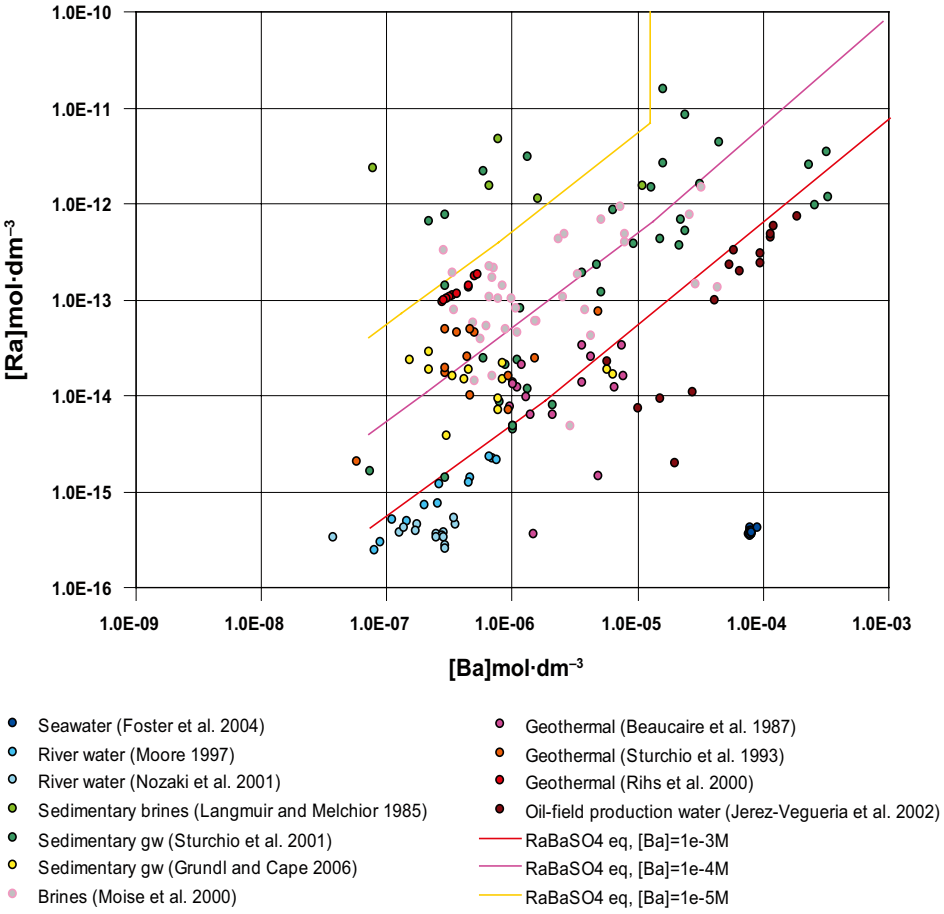

Figure 2-2. *Radium vs barium concentrations in waters from natural and anthropogenic environments. Solid lines show the calculated Ra and Ba concentrations in a mixture of two granitic groundwaters with variable barium and sulphate concentrations ($[Ba_{tot}] = 10^{-3}$ to 10^{-5} M; $[SO_4^{2-}] = 0.1$ to 10^{-4}M, and fixed initial $[Ra_{tot}] = 10^{-10}$). These lines show similar slope in major natural Ra-Ba trends.*

The coprecipitation of radium with barite has been invoked in many studies to account for the measured aqueous radium concentrations in natural environments. In order to rationalise the obvious correlations, we have calculated the Ra and Ba aqueous concentrations resulting from the mixing between 2 groundwaters with variable Ba content (ranging from 10^{-3} to 10^{-5}M) and sulphate (0.1 to 10^{-4}M) concentration, assuming equilibrium with a $BaRaSO_4$ solid solution. The GEMS code was used /Kulik et al. 2004/ for these calculations (see Section 4 and Appendix B for further details of this code). The results are shown in Figure 2-2. The calculated *(BaRa) SO_4 equilibrium lines* have a similar slope for the various data. This would indicate that it is reasonable to assume that a solid solution of constant composition can be the actual solubility limit for radium in these groundwaters.

In addition to Ba-Ra sulphate solid solutions, carbonate solid solutions have occasionally been invoked as solubility limiting phases. /Andrews et al. 1989/ found a correlation between radium and calcium concentrations in Stripa groundwaters, and concluded that $(Ca,Ra)CO_3$ solid solutions could control the radium solubility. However, most groundwaters from Stripa are saturated in barite /Nordstrom et al. 1989/ so that it is likely that $(Ba,Ra)SO_4$ solid solutions may have some solubility control on radium.

In the Poços de Caldas analogue study the radium content in the rock was measured across the well characterised redox front. The measured profile is shown in Figure 2-3. The increase of radium content is noticeable from the oxidised area towards the redox front, as well as the sharp decrease in the reduced part of the front. This was explained by /McKenzie et al. 1993/ as the result of the association of Ra(II) with the active redox couples in the system (Fe(III)/Fe(II) and SO_4^{2-}/S^{2-}). While no further characterisation was performed it is tempting to hypothesise that Ra(II) was associated with sulphate in the oxidised zone and released when sulphate was reduced to sulphur. This could be an indication of the vulnerability of $BaRaSO_4$ solid solutions to reducing conditions.

In the Cigar Lake Analogue Project /Cramer and Smellie 1994/ ^{226}Ra was measured in the sampled groundwaters during the project work (Figure 2-4). The measured data did not show a clear orrelation with the measured Ba(II) concentrations, particularly those waters sampled close to the central part of the ore deposit which had the largest ^{226}Ra content (4.3 Bq L^{-1}). This could be the result of the prevalent reducing conditions close to the ore.

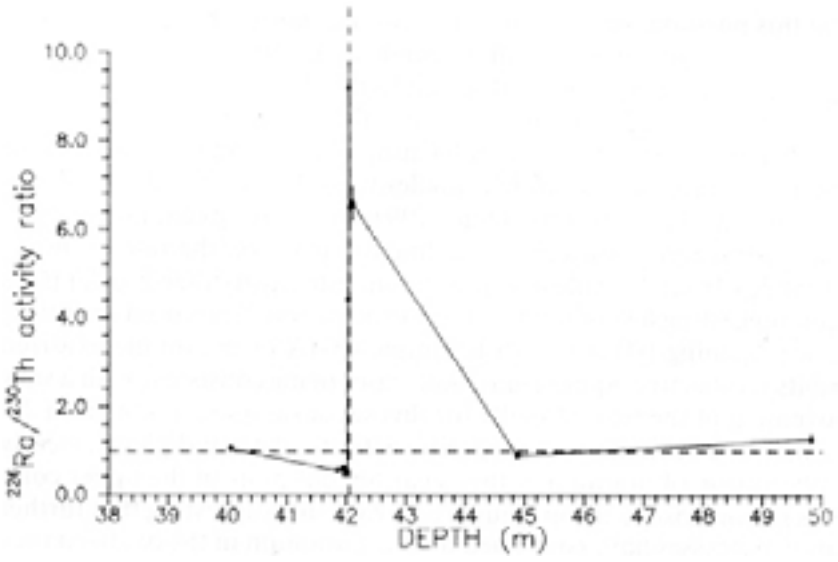

Figure 2-3. *$^{226}Ra/Th^{230}$ activity ratios for the transect samples across the 42.0 m redox front at the Otsamu Usumi uranium mine in Poços de Caldas /McKenzie et al. 1993/.*

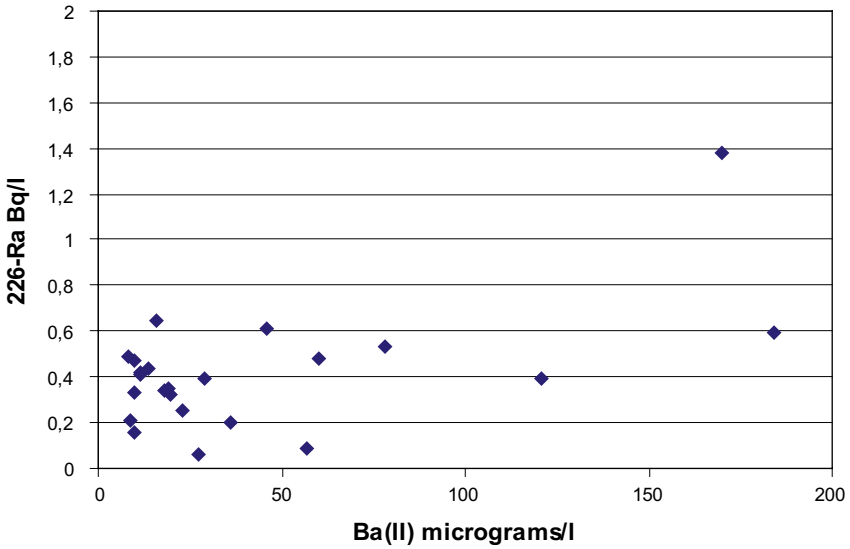

Figure 2-4. *^{226}Ra vs Ba(II) in the sampled groundwaters at Cigar Lake /Cramer and Smellie 1994/. The sampled groundwaters in the core of the ore (220A and 220B) showed ^{226}Ra content up to 4.3 Bq/l while Ba(II) concentrations where in the 35 micrograms range.*

2.4 Formation of (Ba,Ra)SO_4 in anthropogenic environments

Oil fields

The formation of (Ba,Ra)SO_4 solid solution (known as radiobarite in the oil exploration jargon) is ubiquitous in oil production environments (e.g, /Kraemer and Reid 1984, Smith 1987, Wilson 1994, Fisher 1998, Hamlat et al. 2003, Al-Masri and Suman 2003/). The precipitation of radiobarite is triggered by changes in the chemical composition of the production waters. Production waters are the result of mixing formation waters and the waters injected during oil extraction operations (e.g. /Sorbie and Mackay 2000/). They can contain relatively large concentrations of dissolved Ra(II) (10 to 10^3 pCi/L, /Fisher 1998/. /Kraemer and Reid 1984/ reported a quick decrease in the ^{226}Ra activity in production waters in the Gulf Coast region, which was caused by precipitation of (Ba,Sr,Ra)SO_4 due to the decrease in temperature from 100°C to 20°C. (Ba,Ra)SO_4 solid solution precipitates in oil industry equipment forming crusts known as scales (Figure 2-5) and can be a significant source of radioactivity (up to 1×10^3 Bq·g^{-1}). Consequently, it has been considered as a Technologically Enhanced Naturally Occurring Radioactive Material (TENORM). Experimental studies have been performed to minimise the potential risk of these (Ba,Ra)SO_4 precipitates. Recently, /Ceccarello et al. 2004/ investigated the effect of Sr^{2+} ions on the incorporation of radium in the barite structure. They concluded that radium uptake depended on the degree of supersaturation with respect to celestite during the nucleation and growth of barite crystals, and that high Sr/Ba initial ratios in the solution significantly lowered the incorporation of radium in the solid solution. This is in contradiction with the observations made by /Goldschmidt 1938/ previously discussed.

Uranium milling tailings

Another potential source of information regarding the coprecipitation of Ra(II) with Ba(II) sulphate arises in the front end of the nuclear cycle. Elevated concentrations of radium (as high as 1×10^{-11} mol·L^{-1} /Sebesta et al. 1981/ are found in leachates from uranium mill tailings, which have a substantial acidity. Many studies have indicated that the solubility of radium in these waters is commonly controlled by coprecipitation with barite /Benes 1984, Snodgrass and Hileman 1985, Martin and Akber 1999/. In the uranium mining industry, uranium is usually concentrated from ore minerals by dissolution, frequently with sulphuric acid. During this operation, some radium remains insoluble in the fine fraction of the waste, which is finally

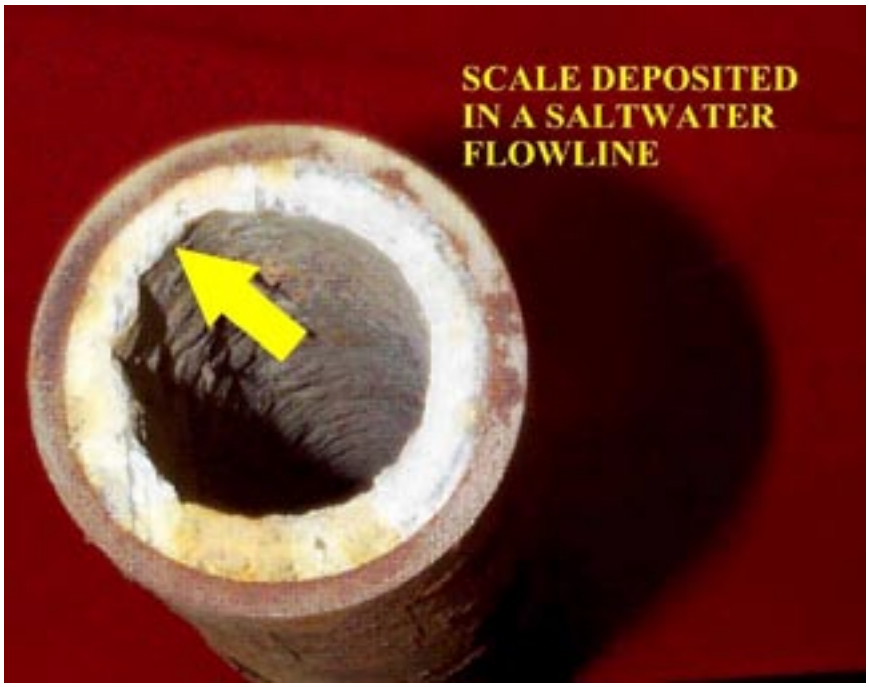

Figure 2-5. *Barite scale in pipe from an oil field in Mississippi (USA).*

deposited in tailings. Radium(II) can be mobilised from these tailings under some environmental conditions. /Martin et al. 2003/ showed that radium mobility in mill tailings was limited in oxic environments due to the formation of $(Ba,Ra)SO_4$ solid solutions, but microbial activity in deeper, anoxic zones of the tailings could destabilize this solid solution by reduction of sulphate to sulphide resulting in the release of radium to the soil. Microbially-assisted dissolution of $(Ba,Ra)SO_4$ had already been observed in laboratory experiments performed by /McCready et al. 1980, Fedorak et al. 1986/.

A common practice to reduce radioactivity in uranium tailings waters in order to avoid contamination to surface and groundwaters is the addition of $BaCl_2$ to enhance $(Ba,Ra)SO_4$ precipitation /Sebesta et al. 1981, Huck et al. 1989/. Sulphate concentrations are typically in excess so that the addition of barium is the only requirement to guarantee solid solution formation. A good example of this practise was reported by /Sebesta et al. 1981/ who studied the effect of $BaCl_2$ addition to waste waters from uranium mining tailings in the Czech Republic. They observed a large reduction of the amount of dissolved radium, and established that more than 92% of the dissolved radium was precipitated as $(Ba,Ra)SO_4$ solid solution as a result of the addition of Ba(II).

Phosphoric acid manufacturing

The manufacturing of phosphoric acid commonly leads to radium-rich by-products. During the manufacturing procedures, high-levels of natural uranium-series radionuclides are transferred from the original phosphate ore to these by-products. Their high radioactivity can prevent the further use of these materials. One of these by-products is phosphogypsum, which can reach ^{226}Ra contents up to 2,000 $Bq \cdot kg^{-1}$. The production and storage of phosphogypsum is a potential risk for radionuclide release to natural environments, and many studies have been developed to characterise phosphogypsum tailings (e.g. /Rutherford et al. 1996, Burnett and Elzerman 2001, Beddow et al. 2006/). In some cases, hydrochloric acid instead of sulphuric acid is used for phosphate-rock leaching in phosphoric manufacturing process use. In this instance, no phosphogypsum is produced and $CaCl_2$-rich effluents with high contents in ^{226}Ra are mobilised, and, eventually, discharged into surface waters /Paridaens and Vanmarcke 2001/. The treatment commonly used to reduce radium levels is the addition of $BaCl_2$ and Na_2SO_4 to precipitate $(Ba,Ra)SO_4$ solid solutions.

2.5 Stability of $(Ba,Ra)SO_4$ solid solution

The capacity of $BaSO_4(s)$ to retain radium via coprecipitation and solid solution formation not only lies in the ability to precipitate the solid solutions but also in the stability of the precipitated solid solution phases. Changes in the chemical composition of the contacting fluids of the system could render unstable the newly-formed $(Ba,Ra)SO_4$ phase with the subsequent release of radium(II) back into the aqueous phase.

The stability of $(Ba,Ra)SO_4$ solid solutions has been mainly discussed in connection with uranium mining tailings (e.g. /McCready et al. 1980, Fedorack et al. 1986, Huck et al. 1989/), and in scales in the oil industry equipment /Phillips et al. 2001/ (see Section 2.4 above). From these studies, two main processes are believed to cause re-dissolution of $(Ba,Ra)SO_4$ solid solutions:

1. acidification (pH < 3) or alkalinisation (pH > 12), and
2. bacterially promoted sulphate reduction.

/McCready et al. 1980/ studied the solubility of $(Ba,Ra)SO_4$ precipitates from uranium mine tailings in the pH range (2 to 10) and $[SO_4^{2-}]_T$ (from 2.6×10^{-3} to 0.156 $mol\cdot L^{-1}$, at temperatures of 5 and 25°C. They found that the release of radium at 25°C was positively pH-dependent. At 5°C, varying radium releases were observed depending on pH and $[SO_4^{2-}]_T$. At low sulphate concentration ($[SO_4^{2-}]_T= 2.6\times10^{-3}$ $mol\cdot L^{-1}$), a peak of radium release is observed a pH=8. Similar conclusions were reported by /Huck et al. 1989/, who determined the destabilisation of $(Ba,Ra)SO_4$ at pH range from 1 to 13, and concluded that Ra-Ba precipitates were unstable at pH conditions under 3 or over 11.

In addition, laboratory experiments have shown that bacterial activity is able to dissolve $(Ba,Ra)SO_4$ relatively quickly by promoting reducing conditions if organic matter is available to allow microbial growth (e.g. /McCready et al. 1980, Fedorak et al. 1986, Phillips et al. 2001/). This process has implications in the radium retention capacity of uranium tailings, since they may progressively become anoxic promoting SRB (sulphate reducing bacteria) activity. /McCready et al. 1980/ also carried out experiments to determine the effect of sulphate-reducing bacteria on $(Ba,Ra)SO_4$ stability and they concluded that SRB activity can significantly accelerate the dissolution of barium and radium sulphate solid solution. Barium was, however, re-precipitated as $BaCO_3(s)$ due to the production of CO_2 by metabolic activity.

In terms of the processes to be discussed in this report, it is clear that the destabilisation by acidification can be disregarded as none of the scenarios explored in SR Can indicates that low pH waters would reach the near field. High pH values in the contacting fluids can only be the result of the infiltration of cement waters in the near field. This is an unlikely event, but it will have to be considered in the definition of the limits for the application of the conditional solubility limit for Ra(II).

Sulphate reducing bacteria (SRB) will only reach the vicinity of the fuel if the density of the compacted bentonite is lower that 1.6 kg/m^3 and the corresponding water activity becomes close to unity /Motamedi et al. 1996/. However, it is highly unlikely that SRB's will survive the radiation field in the vicinity of the fuel. Nevertheless, sulphate concentration limits will be defined in the establishment of the conditional solubility limit for Ra(II).

2.6 Thermodynamic modelling of the (Ba,Ra)SO_4 aqueous/solid solution system

The analysis of the thermodynamic equilibrium between aqueous solutions and solid solution (SSAS) has been done by a number of approaches. The most accepted method is the *total solubility product* $\Sigma\Pi_{eq}$, proposed by Lippmann in a series of pioneering papers /Lippmann 1977, 1980, 1982/. Its applicability was later demonstrated by Glynn and co-authors (/Glynn and Reardon 1990, Glynn et al. 1990, Glynn 2000/). The first computer-aided code for calculating SSAS was based on Lippmann's concepts (MBSSAS code, /Glynn 1991/). Later, the Lippmann approach was extended by /Gamsjäger et al. 2000/ in the so-called *unified theory of solid solution solubility*. The thermodynamic equilibrium of this approach to study aqueous solid solution (SSAS) systems is based on law-of-mass action equations, and it is explained in detail in the Appendix A of this report.

/Kulik et al. 2000/ developed a different approach to model SSAS systems: the *Gibbs energy minimisation (GEM) approach*. In this method, calculations of thermodynamic equilibrium are based on the concept of chemical potential equality of a component in all co-existing phases established by Gibbs. It has proved to be very useful for (1) computing equilibrium partitioning between solid and aqueous solutions, (2) retrieving unknown activities of solid solution end members, and (3) estimating activity coefficients in non-ideal solid solution systems. More details of GEM methodology are given in Appendix B.

The quantitative modelling of radium retention by (Ba,Ra)SO_4 solid solutions has been recently developed using codes based on the mass-action-law or the Gibbs energy minimisation. /Berner and Curti 2002/ performed a detailed study of the decrease of the solubility limit for radium in the near field. They calculated the total mole amount of barium and strontium existing in the bentonite mass (rock and porewater) per one canister, and the total mole amount of radium in a spent fuel per canister after 300,000 years of storage. Using the GEM-PSI code (see Appendix B), they estimated the solubility limit of radium in the clay porewater considering both the "conventional" approach, i.e. the total concentration of dissolved radium being controlled by the least soluble pure phase ($RaSO_4$(s)), and the formation of (Ba,Ra)SO_4 solid solutions. The calculations were made considering the entire system as a batch experiment, i.e. all moles of the reactive elements were "mixed" together and dissolved in a porewater volume of ~ 1.3×10^4 litres, which is the amount of water in bentonite corresponding to one canister. Conceptually, this means that all radium produced in the spent fuel is immediately released and homogeneously dissolved into the porewater containing barium. This approach is not very realistic since the radium inventory is not instantaneously released. In addition, the water volume involved in spent fuel dissolution is much smaller, so that radium concentrations could be much higher. Another point that is not taken into account is the barium inventory already existing in the spent fuel that can be released during dissolution, so that solid solution precipitation can occur in the fuel gap just after the intrusion of porewater. The results reported by /Berner and Curti 2002/ are, despite these considerations, illustrative of the capacity of solid solutions to substantially reduce the radium aqueous concentration. In their approach, radium concentration was lowered by more than 3 orders of magnitude, from 4.8×10^{-8} mol·L^{-1} in the case of $RaSO_4$ equilibrium to 8.6×10^{-12} mol·L^{-1} when solid solutions were considered.

/Zhu 2004b/ modelled the co-precipitation and co-dissolution of (Ba,Ra)SO_4 solid solutions in a hydrodynamic environment, using reactive transport codes based on the law of mass action (EQMOD and PHREEQC). In one of these model calculations, he was able to simulate the radium incorporation into barite structure during scale precipitation in enhanced oil recovery processes. Barite precipitated due to cooling of the solution from 100°C to 25°C, and radium was calculated to be readily removed from the solution, resulting in that only a small fraction of the initial aqueous radium remained in solution (from ~ 5×10^{-10} mol·L^{-1} to ~ 1×10^{-13} mol·L^{-1}). During the precipitation process, the solution was far from saturation with respect with pure $RaSO_{4\,(c)}$, and degree of saturation ranged between 10^{-5} and 10^{-7}.

3 Time evolution of Cs, Ba and Ra

It is clear from the previous discussions that the formation of a $(Ba,Ra)SO_4$ (ss) depends on the contemporaneous availability of Ba(II) and sulphate as ^{226}Ra is released from the primary and secondary sources (direct release from the spent fuel matrix and release from the secondary precipitated UO_2(s)).

It is, therefore, quite important to establish the time windows in the repository lifetime when this could occur.

3.1 Unaltered spent fuel

We have carried out a first calculation of the intrinsic evolution of element inventories in the spent fuel assuming that the fuel remains unaltered during the whole period of interest (10^6 years). The spent fuel considered has been the testing material ATM-104 with a burnup of 40 MWd/kgU /PNL 1991/, The reason for using this fuel as an example instead of the SKB fuel in /Håkansson 1999/ is that inventory data for stable barium is missing in the /Håkansson 1999/ report. This fuel is considered to have similar characteristics to the Swedish reference fuel (Spahiu, pers. comm.) and the reported inventory contains data on barium content. We have taken the isotope inventory on a g/gU basis at 4 years after discharge, and calculated its time evolution with the Amber software package /Amber 2006/. The whole actinide series has been included to properly account for radioactive in-growth of radium. The result of this calculation is given in Figure 3-1 and Figure 3-2. We can see from Figure 3-1 how the main composition of barium as an element is initially given by the content of the stable isotope ^{138}Ba. After 200 years of evolution the total amount of barium has nearly doubled due to ingrowth from ^{137}Cs to ^{137}Ba. Finally, at the end of the simulation (10^6 years), a slight increase in barium is observed due to decay of ^{135}Cs to ^{135}Ba.

The total content of barium in the spent fuel is dependent on the burn-up of the fuel. However, since the canisters are designed for a certain residual power (1,700 W in SR-Can) and the residual power is strongly dependent on the content of Cs-137 the variability of the barium content in the canisters can be expected to be rather limited, although the residual heat could, in principle, be reduced by long-term cooling with the subsequent reduction of barium content.

The time evolution of the radium content is the result of the ^{238}U and ^{234}U decay chains (Figure 3-2, top). The time evolution of the radium to barium molar ratio has been calculated and it is plotted in Figure 3-2 (bottom). From an initial value of ca 10^{-10}, the Ra/Ba molar ratio may increase up to 2×10^{-4} after some 10^5 years. These are expected ratios in the fuel if according to the pinhole defect scenario water gets in contact after a few thousand years. The main inventories of ^{226}Ra and other dose contributing radionuclides are given in Table 3-1, which is taken from Table 10-4 of the SR-Can main report /SKB 2006a/.

Table 3-1. Inventories (Bq) in one canister of the most important radionuclides at 300,000 years for different fuel types and burn-up (MWd/kg U). From /SKB 2006a/.

	BWR 38	PWR 42	BWR 55	PWR 60
Ra-226	9.3×10^{10}	8.9×10^{10}	8.9×10^{10}	8.6×10^{10}
Th-229	7.0×10^{10}	7.7×10^{10}	5.3×10^{10}	5.6×10^{10}
Th-230	9.3×10^{10}	8.8×10^{10}	8.8×10^{10}	8.6×10^{10}
I-129	2.6×10^{9}	2.5×10^{9}	2.4×10^{9}	2.3×10^{9}

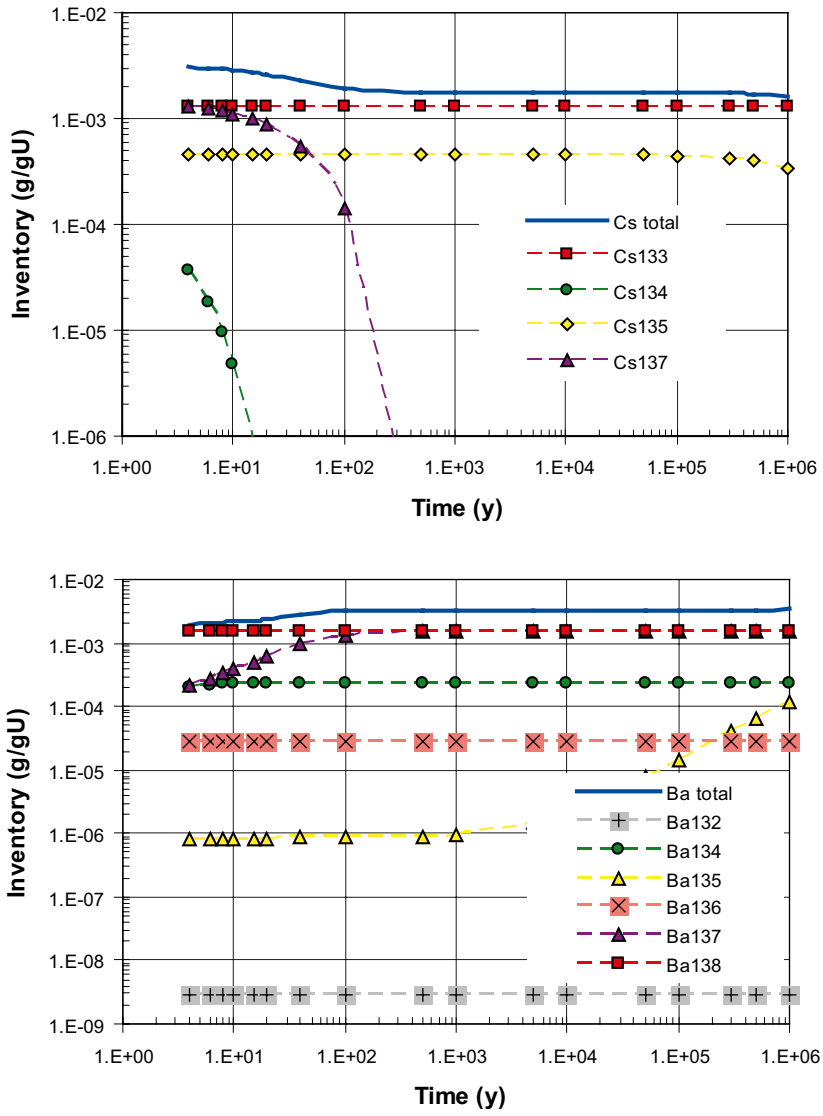

Figure 3-1. *Time evolution of caesium and barium in unaltered spent fuel.*

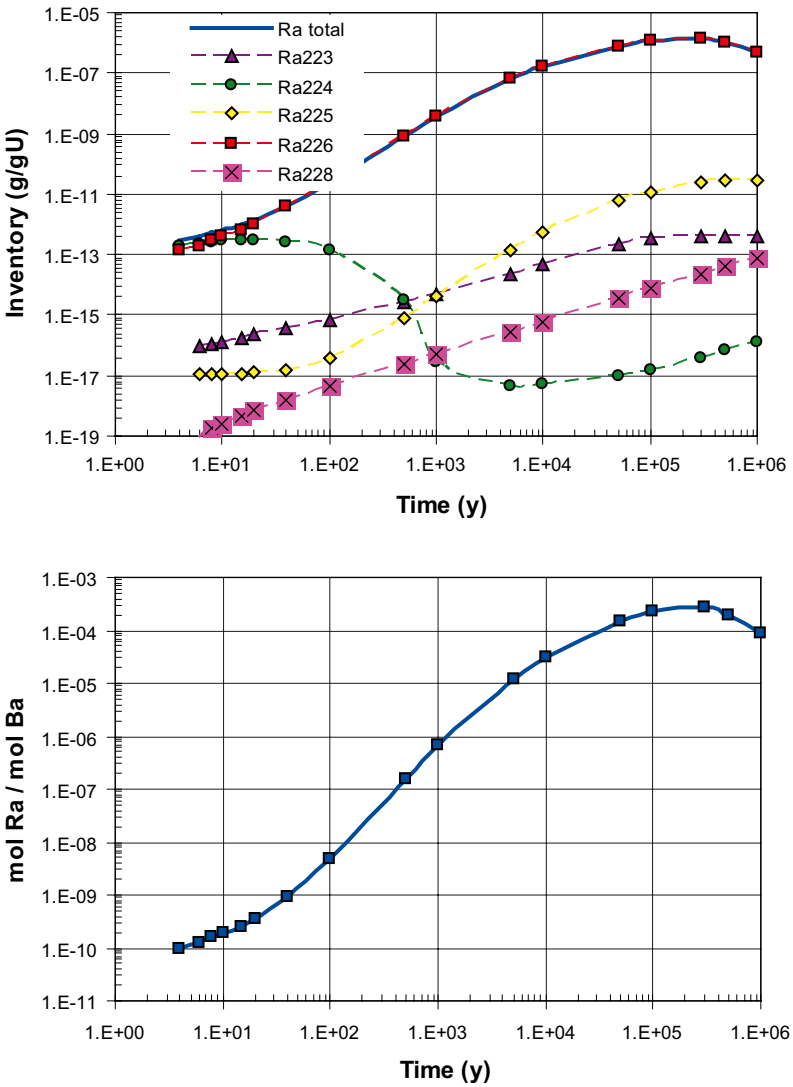

Figure 3-2. *Top: Time evolution of radium in unaltered spent fuel. Bottom: Time evolution of the molar ratio between Ra and Ba in unaltered spent fuel.*

4 Scoping geochemical calculations

4.1 Current approach in performance assessment

The material balances in the vicinity of the spent fuel elements are handled according to the Comp23/Nuctran users guide /Romero et al. 1999/ as follows:

In order to take into account the evolution of the solid inventory, the spent fuel physical compartment is fictitiously divided into two subcompartments, one that handles the solid inventory and another one that takes into consideration the released components, either dissolved in water of sorbed in the solid materials. An additional compartment is used to include the amount of radionuclides embedded in the fuel matrix. The mass balance in the vicinity of the fuel is affected by: the spent fuel dissolution rate, the decay rates and the accumulation of the dissolved species in the aqueous compartment. In Comp23/Nuctran /Romero et al. 1999/ the embedded radionuclides are liberated as the $^{238}UO_2$(s) fuel matrix dissolves and they are assumed to dissolve congruently with the ^{238}U content. The nuclide inventory in the canister can be found in three states: embedded in the fuel matrix, precipitated as secondary solids and dissolved in the water volume. The radionuclide content in the dissolved fraction is limited by the individual solubility limit; when this is reached the radionuclide is transferred to the secondary solid state.

The calculation of the individual solubility of the radionuclides in the vicinity of the spent fuel element is calculated according to the principles stated in /Duro et al. 2006/. The main conceptual uncertainty in these calculations is related to the selection of the solubility limiting solid phases in the canister conditions. The strategy for the solid phase selection is based on expert judgement, which is very dependent on the knowledge about the composition of the contacting waters, the kinetics of the processes involved and in the relevant analogies. As a general principle the solubility limiting phases are assumed to be individual solid phases, which are expected to be thermodynamically stable and kinetically favourable in the conditions expected in the vicinity of the disposed fuel elements. For ^{226}Ra the expected solubility limiting phase is assumed to be $RaSO_4$(s), which is both kinetically and thermodynamically expected to precipitate in the near field. However, from the point of view of relevant natural and anthropogenic analogies and as we have already discussed, $RaSO_4$(s) has never been identified, while the formation of Ra(II) Ba(II) sulphate solid solutions is ubiquitous.

4.2 Thermodynamic properties of alkaline earths used in calculations

Thermodynamic data for radium have been extrapolated from data of similar alkaline earth elements, mainly calcium, strontium and barium. /Langmuir and Riese 1985/ compiled the most complete thermodynamic database for radium solids and aqueous complexes. The least soluble individual solid phase that incorporates radium is the normal $RaSO_4$(s). Its solubility in aqueous solution was determined in an early study by /Nikitin and Tolmatscheff 1933/, who provided a value for $\log K_{sp} = 10.38 \pm 0.02$ at 20°C. Recalculation to 15°C gives a constant of $\log K_{sp} = 10.5 \pm 0.1$. In Table 4-1, the thermodynamic data for radium aqueous species and solid phases used in the calculations in Section 4.4 are listed. Solubility constants for barite and celestite, which are the other alkaline earths sulphates assumed to be involved in radium coprecipitation, are $10^{-9.97}$ (from /Blount 1977/) and $10^{-6.63}$ (from /Struebel 1966/) at 25°C.

Table 4-1. Log K values for radium aqueous species and solid phases at 15°C used in the calculations. Data from /Langmuir and Riese 1985/.

Reaction	log K_f	ΔH^o (kcal·mol^{-1})
aqueous species		
$Ra^{2+} + OH^- \leftrightarrow RaOH^-$	0.50	1.10
$Ra^{2+} + Cl^- \leftrightarrow RaCl^-$	-0.10	0.50
$Ra^{2+} + CO_3^{2-} \leftrightarrow RaCO_{3aq}$	2.50	1.07
$Ra^{2+} + SO_4^{2-} \leftrightarrow RaSO_{4aq}$	2.75	1.30
solid phases	log K_{sp}	
$RaCO_3 \leftrightarrow Ra^{2+} + CO_3^{2-}$	-8.30	-2.80
$RaSO_4 \leftrightarrow Ra^{2+} + SO_4^{2-}$	-10.26	-9.40

4.3 Conceptual model

The calculations made in this study are based on the hypothesis that the formation of $(Ba,Ra)SO_4$ solid solutions occurs inside the canister when, as a consequence of failure of canister integrity, a sulphate-containing water dissolves the Ba(II) and Ra(II) present in the spent fuel and in the secondary uranium dioxide precipitate (Figure 4-1) considering that, as indicated by the calculations shown in Figure 3-2 bottom, the relative amount of Ra(II) will be at most 1,000 times or more lower than the Ba(II) content.

The ultimate objective of these preliminary calculations is to evaluate the effect of Ra-Ba co-precipitation on the radium solubility limit by taking into consideration the thermodynamics of solid solution formation,

$(Ba,Ra)SO_4$ solid solution precipitation is mainly controlled by eight different parameters:

1. sulphate concentration
2. radium concentration
3. barium concentration
4. accessible volume of water
5. fuel alteration rate
6. composition of the solid phase
7. temperature
8. transport out of species

The variability of these parameters is discussed in the next paragraphs.

Evolution of sulphate concentration in the canister

The concentration of sulphate is a key factor controlling the extent of radium incorporation in $(Ba,Ra)SO_4$ solid solutions and it can be highly variable in both temporal and spatial scales. After the disposal of the waste-containing canister in the deposition hole, groundwater starts to saturate the bentonite pores, reacting with existing accessory minerals. Bentonite rocks, including those envisaged to be used as engineered barriers in a HLNW repository (MX-80 and Deponit Ca-N), contain minor amounts of sulphate minerals, mainly gypsum and/or anhydrite /SKB 2006a/. Most groundwaters are undersaturated with respect to these minerals and, consequently, the water saturation of bentonite implies the net addition of sulphate to the bentonite porewater. It is worth remembering that the solubility of calcium sulphate minerals is not only determined by the aqueous sulphate concentration but also by the concentration of calcium, which in turn is controlled by ion exchange processes in the clay fraction and by dissolution/precipitation of other Ca-bearing solids such as calcite and dolomite.

The evolution of porewater chemistry in the near field of a HLNW repository has been evaluated by /Arcos et al. 2006/. The reactive transport simulations showed that gypsum (with an initial pore water content of 1.27 mol L^{-1}_{pw}) is readily dissolved from the bentonite in response to the inflow of Forsmark-type groundwater (Figure 4-2).

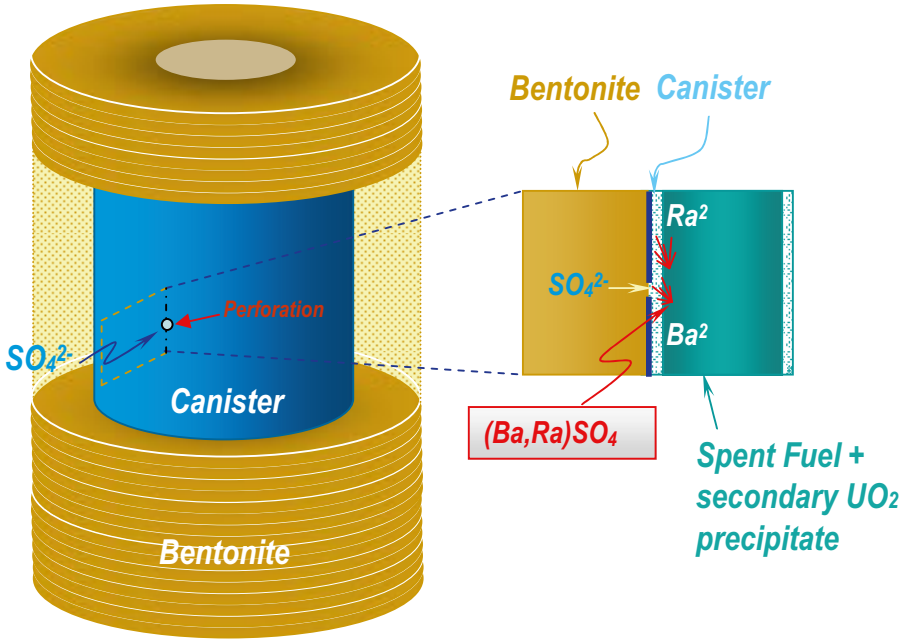

Figure 4-1. *Conceptual model of Ra co-precipitation with barium sulphate. SO_4^{2-} ions from porewater contacting spent fuel through a perforation in the canister. Barium and radium in the fuel are leached and subsequently immobilised via solid solution formation.*

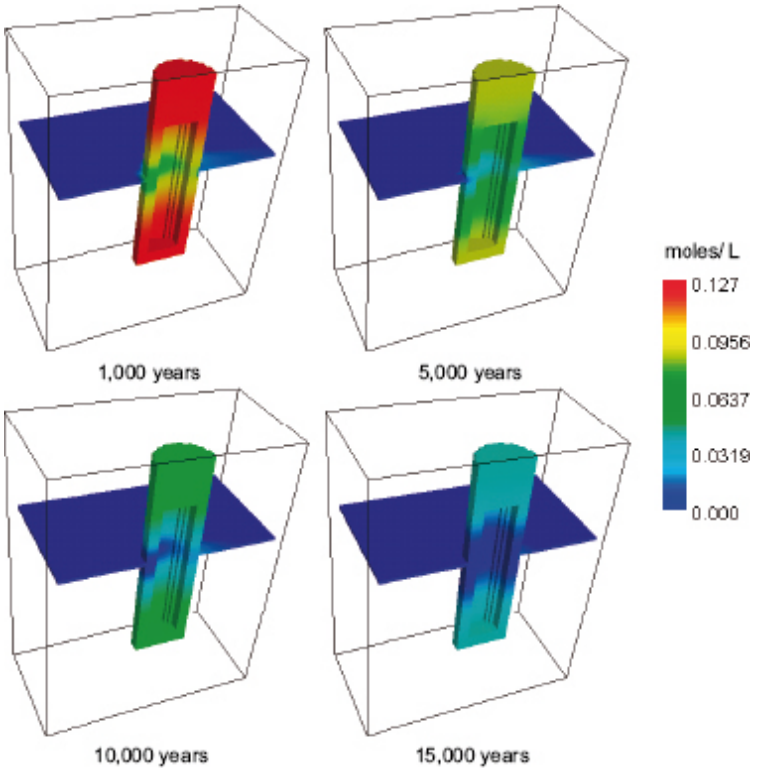

Figure 4-2. *Simulated dissolution of gypsum in bentonite barrier after 15,000 years of interaction with a Forsmark-type groundwater (from /Arcos et al. 2006/).*

The dissolution of gypsum is significantly enhanced if highly diluted waters intrude into the system. Figure 4-3 has been drawn from the modelling results obtained in /Arcos et al. 2006/. It shows the evolution of sulphate and gypsum concentrations in the canister-bentonite contact when ice-melting water (Grimsel type) replaces the granitic groundwater. After the intrusion, calcium concentration is largely depleted so that sulphate concentration is increased to maintain the equilibrium with gypsum (up to 4×10^{-2} mol·L^{-1}). In bentonite sections close to the fracture, gypsum is completely dissolved in the following 600 years after the contact and, thereafter, sulphate concentration decreases rather quickly down to levels found in the ice-melting-water (6×10^{-5} mol·L^{-1}). In sections far from the fracture (see Figure 4-3), the time for total removal of gypsum can be up to 3,000 years. The disappearance of accessory gypsum and the decrease of the dissolved sulphate are not directly coupled due to the equilibrium with calcite and Ca-exchange reactions within the clay.

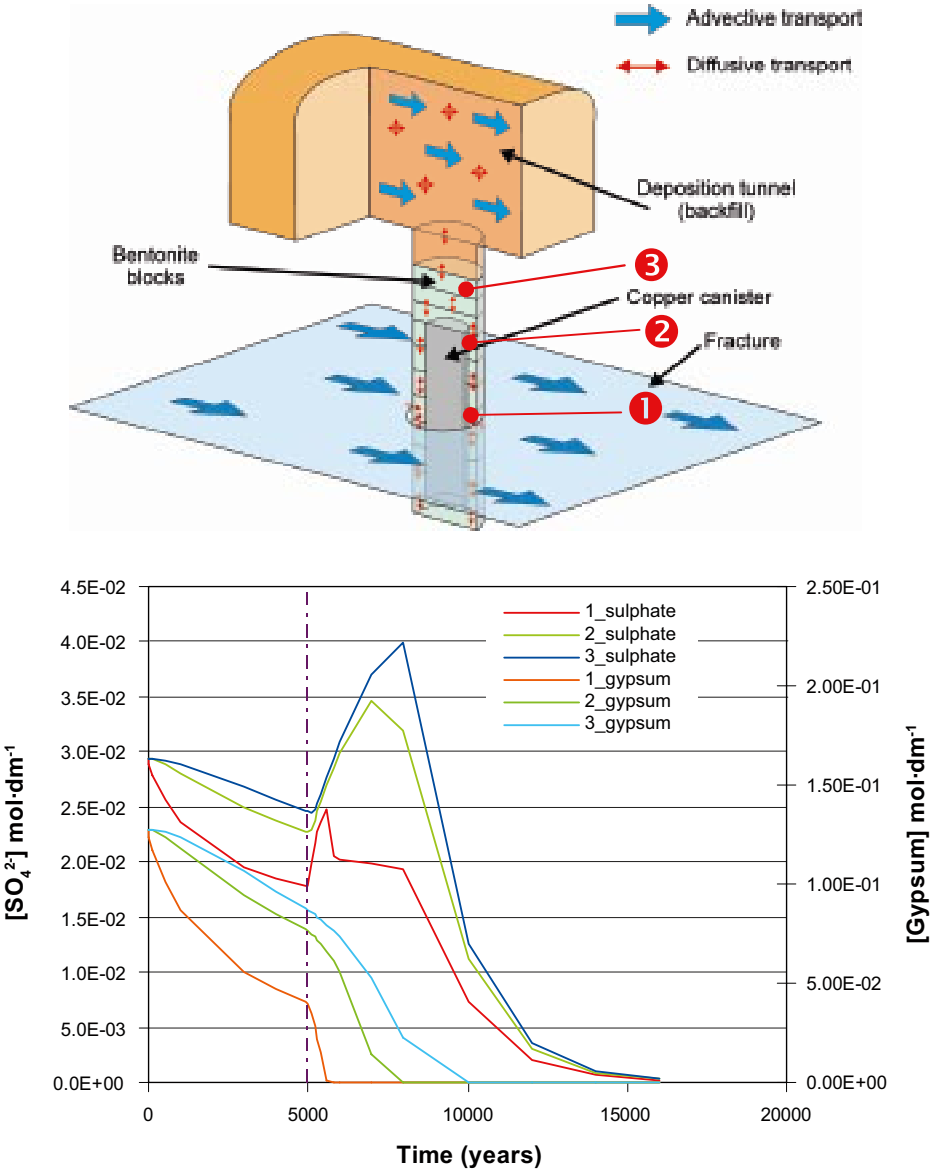

Figure 4-3. *Evolution of sulphate and gypsum concentrations in bentonite porewater close to the canister in three points located at different distances from the fracture (see near field sketch). Granitic, Forsmark-type groundwater is replaced by ice-melting water after 5,000 years (vertical, dashed line). In this simulation, waters only flow into the bentonite barrier from the fracture. Modified from /Arcos et al. 2006/.*

The variability of the sulphate concentration in natural groundwaters in the Fennoscandian shield is well illustrated in Table 9-23 in the Sr-Can Main Report /SKB 2006a/. The expected sulphate concentration ranges from 1×10^{-6} to 9×10^{-3} mol·L^{-1}.

From this discussion it can be concluded that the range of $[SO_4^{2-}]$ in water that may be in contact with spent fuel in case of canister failure is rather variable and depends on the nature of the flowing groundwater and the initial inventory of accessory calcium sulphate minerals in the bentonite.

Ba(II) solubility in the near field

Ba(II) is not a relevant radionuclide *per se*, in terms of its radiological consequences; therefore it has not been considered in the recent radionuclide solubility calculations /Duro et al. 2006/. However, Ba(II) solubility is critical in order to establish the potential occurrence of Ra/Ba coprecipitation and its effect on Ra(II) solubility.

As already pointed out, the solubility behaviour of Ba(II) is mainly connected to the relative content of sulphate and carbonate in groundwaters. This is exemplified by the predominance diagram of the Ba(II) solid phases shown in Figure 4-4.

The diagram shows that for most of the expected sulphate/carbonate concentration ranges in granitic groundwaters, $BaSO_4$(s) will be the solubility limiting phase for Ba(II). Only in sulphate diluted groundwaters with carbonate concentrations in the milimolar range could $BaCO_3$(s) be the solubility limiting phase.

In the expected concentration range of dissolved Ba(II) in equilibrium with barite, the aqueous speciation will be mainly dominated by the free cation and the $BaSO_4$(aq) complex only occurs at moderately to high sulphate concentrations (Figure 4-5).

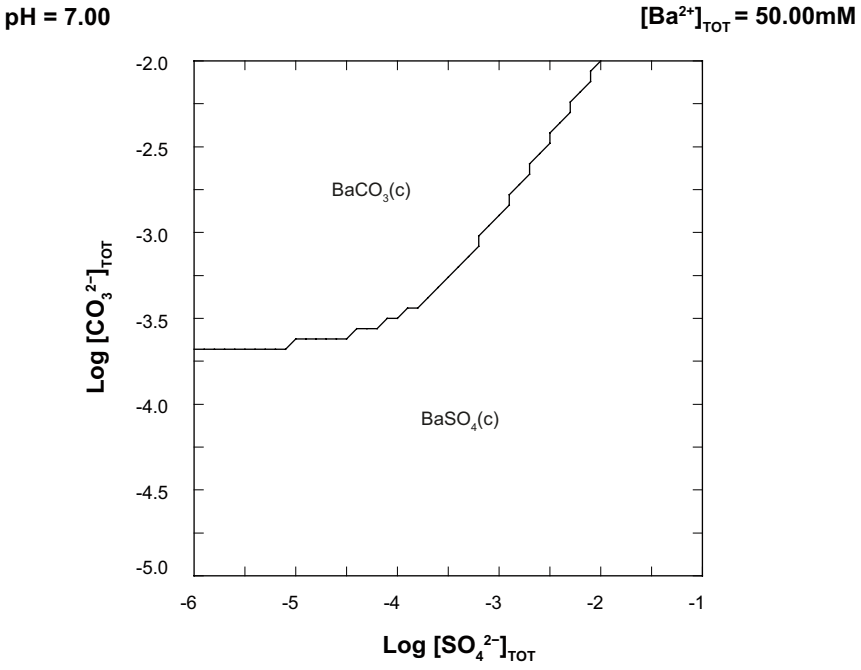

Figure 4-4. *Predominance diagram of the Ba(II)-sulphate-carbonate system at high Ba(II) concentration, at pH 7 and under oxidising conditions.*

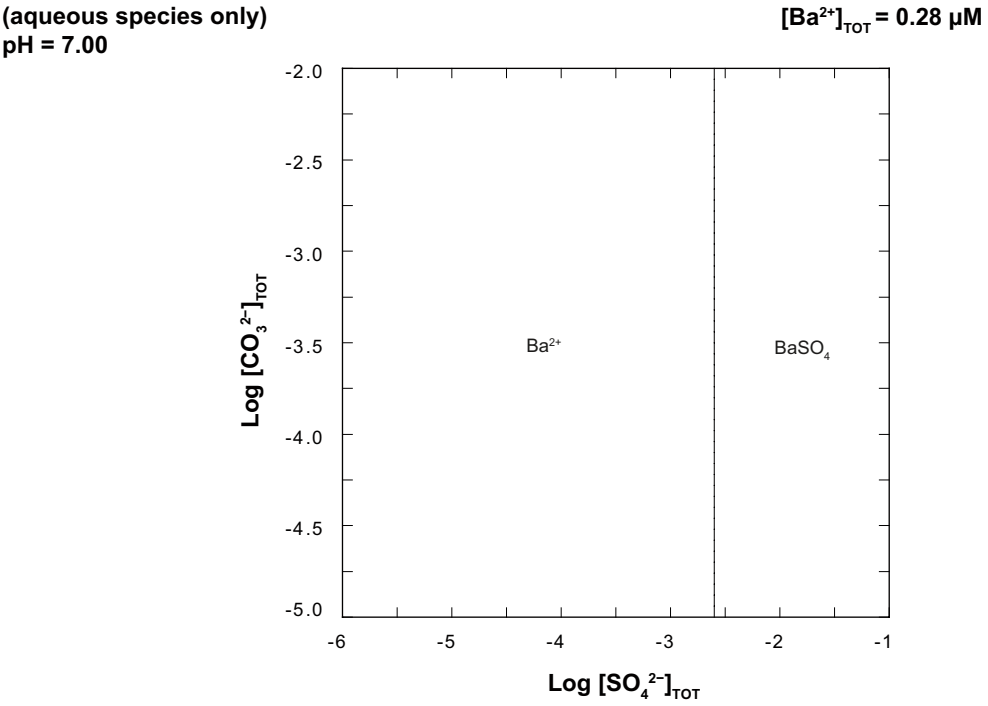

Figure 4-5. *Predominance diagram of the aqueous Ba(II)-sulphate-carbonate system in equilibrium with $BaSO_4$(s), at pH = 7.*

Radium and barium content in the canister

In Section 3.1 we have discussed the time evolution of barium and radium in the canister. The main outcome of this discussion is that the Ba(II) content is at least 1,000 times larger than the Ra(II) content in the canister and therefore the relative amounts of Ra(II) to Ba(II) are always guaranteed to sustain the coprecipitation process.

The time evolution of the dissolved Ra(II) and Ba(II) in 1 m^3 of contacting water filling the canister is given in Figure 4-6.

In the previous sub-section the Ra/Ba ratios have been calculated by assuming that there is no interaction of the fuel with the surrounding environment. Obviously, spent fuel must be altered (corroded) in order to render possible the transfer radionuclides from the UO_2 matrix to the water available under repository conditions. Furthermore, the solubility calculations based on the solid solution thermodynamics (see next chapter) require as an input the water composition. Therefore, there is a need to use a spent fuel dissolution model in order to ascertain the concentrations of Ba(II) and Ra(II) in the contacting waters. A constant spent fuel dissolution rate with a triangular distribution ranging from 10^{-6} to 10^{-8} y^{-1} and a peak at 10^{-7} y^{-1} is assumed (taken from the spent fuel dissolution model used in SR-Ca, see /Werme et al. 2004/) which applies to all elements present in the spent fuel matrix except the instant release fraction. The total inventories have been estimated taking into account the total mass of uranium per canister, 2.04 tonnes /SKB 2006b/, and the inventories given per gram of uranium in the ATM-104 fuel at 40 MWd/kg U given in the previous section. The volume of water that is available for radionuclide dissolution has been considered to be the free void volume of the whole canister, which is roughly 1 m^3 /SKB 2006c/. We have calculated the time evolution of the Ra(II) and Ba(II) concentrations following one year of contact with the calculated inventories at specific points on time. These are given in Table 4-2.

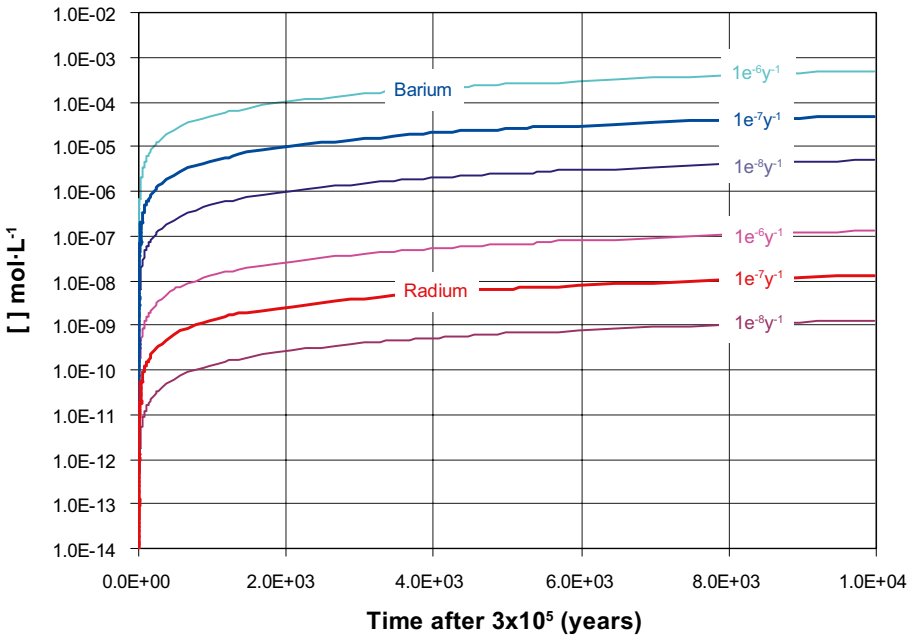

Figure 4-6. *Evolution of barium and radium concentrations in the water filling the free volume of one canister, calculated assuming that no solubility limit is attained. Intrusion is assumed to occur 300,000 years after spent fuel deposition. Reference case considers a spent fuel alteration rate of 1×10^{-7} y^{-1}. Curves showing the concentration at rates of 1×10^{-6} y^{-1} and 1×10^{-8} y^{-1} are also drawn.*

Table 4-2. Concentrations of barium and radium given by the dissolution model. The first column is the time when water enters the system; second and third columns are the evolution of the inventory in the spent fuel. Fourth and fifth columns are the concentrations that Ba and Ra would achieve in 1 year of dissolution after intrusion of water. Concentrations taken in the reference case, see next chapter, correspond to an intrusion time of 300,000 years (boldface).

	Total amount in canister		Predicted concentration after 1 year of dissolution	
Intrusion time (y)	Ba (mol)	Ra (mol)	Ba (mol/l)	Ra (mol/l)
4	29.19	2.81E–09	2.92E–09	2.81E–19
6	30.32	3.85E–09	3.03E–09	3.85E–19
8	31.27	4.87E–09	3.13E–09	4.87E–19
10	32.13	5.92E–09	3.21E–09	5.92E–19
15	33.99	8.82E–09	3.40E–09	8.82E–19
20	35.61	1.24E–08	3.56E–09	1.24E–18
40	40.48	3.64E–08	4.05E–09	3.64E–18
100	46.69	2.24E–07	4.67E–09	2.24E–17
500	48.76	7.69E–06	4.88E–09	7.69E–16
1,000	48.76	3.26E–05	4.88E–09	3.26E–15
5,000	48.77	5.68E–04	4.88E–09	5.68E–14
10,000	48.78	1.47E–03	4.88E–09	1.47E–13
50,000	48.86	7.31E–03	4.89E–09	7.31E–13
100,000	48.96	1.14E–02	4.90E–09	1.14E–12
300,000	49.36	1.29E–02	4.94E–09	1.29E–12
500,000	49.73	9.44E–03	4.97E–09	9.44E–13
1,000,000	50.57	4.55E–03	5.06E–09	4.55E–13

Temperature

The incorporation of radium into a $(Ba,Ra)SO_4$ solid solution is expected to be affected by temperature, as already shown by the experiments of /Gordon and Rowley 1957/ (see Section 2.1). According to the thermodynamic data provided by /Langmuir and Riese 1985/, $RaSO_4$(s) becomes progressively more soluble than barite as temperature increases (Figure 4-7), and these variations would have an influence on the final incorporation of radium in the solid solutions.

In has to be noted that radium inventory in the spent fuel is insignificant just after spent fuel deposition (see section 3), when the maximum predicted temperatures between the bentonite-canister interface and the fuel range between 80 to 110°C /SKB 2006a/. After 5,000–10,000 years, radium accumulated is much higher (between 10^{-5} to 10^{-4} moles per canister), but temperature in the repository is close to that existing before spent fuel deposition (Figure 4-8).

Consequently, the ingrowth of radium is a much slower process than the temperature decrease and the temperature effect on its conditional solubility, assuming coprecipitation with $BaSO_4$(s), can be neglected.

Therefore, in the calculations of solid solution formation performed in the present study the temperature will be set to 15°C.

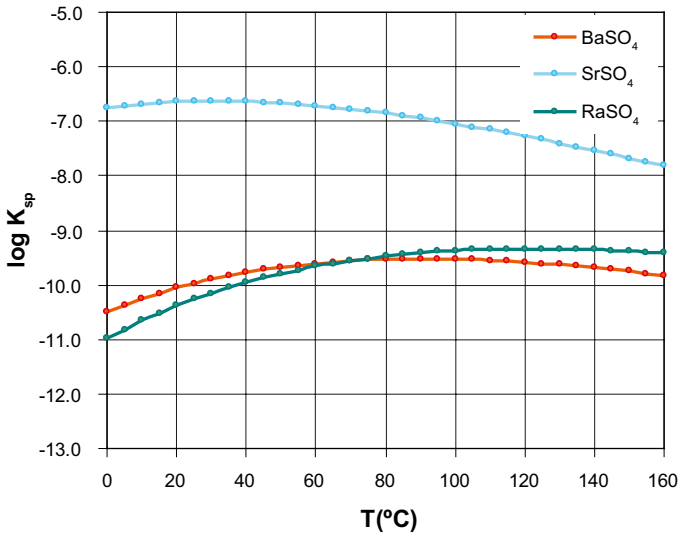

Figure 4-7. *LogK_{sp} vs temperature plot for barite, celestite and $RaSO_{4\,(c)}$, calculated using data from /Blount 1977/, /Struebel 1966/ and /Langmuir and Riese 1985/.*

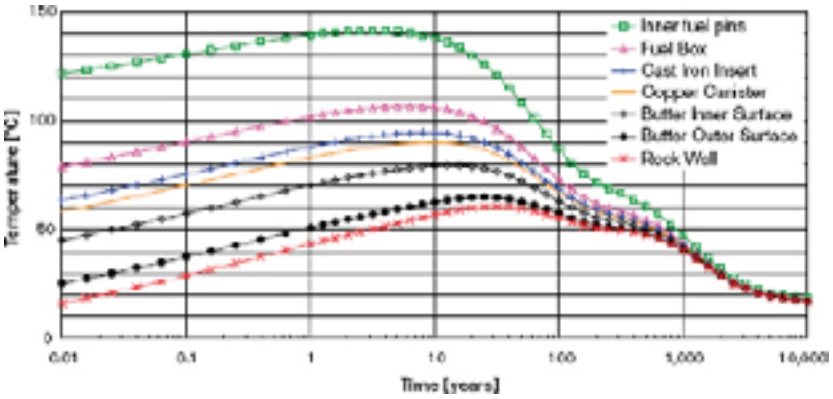

Figure 4-8. *Evolution of temperature in the spent fuel and near field of a HLNW repository (from /SKB 2006a/).*

Composition of the solid solution

It is quite clear from the expected Ra(II) to Ba(II) ratios that the relative amount of Ra with respect to Ba in the precipitating system will be at least 1,000 times lower. Therefore, even in the event of a contemporaneous precipitation (coprecipitation) the relative amount of Ra(II) incorporated in the solid solution will be 1,000 times lower than the actual $BaSO_4$(s) content. As a consequence, the resulting solid solution will contain a relative molar fraction of, at most, $\chi_{Ra} = 0.001$, while χ_{Ba} will be 0.999. Under these circumstances the behaviour of Ra^{2+} in the solid solution is expected to be ideal. This is supported by the fact that the critical parameters to conform an ideal solid solution are /Bruno et al. 2007/.

1. Similarity in size and charge of the host and substituting ions.
2. Similarity in crystal sizes.

Therefore, the low Ra/Ba ratios and the similarity in size/charge and polarizability of the two cations would support treating the Ra/Ba sulphate solid solution as an ideal one.

Transport out of species

Some radium and barium will transported out from the canister according to Section 4.1. This effect is included in the performance assessment modelling, and will not be further investigated in the current study.

4.4 Reference case

Ra content

As a reference case, we have considered that canister perforation and bentonite porewater intrusion take place 300,000 years after spent fuel disposal. The reasons for selecting this timing are: (1) The spent fuel contains the highest Ra/Ba ratio (Figure 3-2-bottom), and (2) Radium production in the spent fuel reaches its maximum (Figure 3-2-top).

Ba-content

After disposal, barium concentration in the spent fuel increases during the first 500 years, and, thereafter, it does not significantly change. Consequently, barium can be considered as constant in our calculations since a water intrusion into the canister can not be expected in the first 500 years. It is worth mentioning that the barium already present in the intruding water is not taken into account in our calculations. This is a conservative assumption since the addition of barium from bentonite would enhance the capacity of the system to form barium-radium solid solutions and, in turn, the radium retention.

Groundwater composition

The groundwater intruding into the canister in the reference case has the chemical composition of the Forsmark granitic water equilibrated with a MX-80 bentonite /Arcos et al. 2006/. This is a neutral porewater (pH=7.08) with an ionic strength of 0.19 M. The main ions are sodium and chloride, with relatively high concentration of sulphate (0.03 $mol \cdot dm^{-1}$). Table 4-3 shows the composition of the major ions in the Forsmark groundwater and in the solution used in the calculation in the present work.

Table 4-3. Composition of porewater that leaches the spent fuel used in the $(Ba,Ra)SO_4$ solid solution calculations. Ion concentrations in $mol \cdot L^{-1}$.

pH	7.08
pe	–2.19
HCO_3^-	2.14×10^{-3}
Ca	9.97×10^{-3}
Cl	1.53×10^{-1}
K	1.14×10^{-3}
Mg	4.97×10^{-3}
Na	1.69×10^{-1}
SO_4^{2-}	2.94×10^{-2}

Properties of the solid phase

Calculations of the solid solution-aqueous solution equilibrium have been performed with the GEMS-PSI code version 2.1.2 /Kulik et al. 2004/. According to the conceptual model assumed in this study, radium and barium are released at a constant rate once the solution is in contact with the spent fuel. The concentration of these elements in the water volume increases until the saturation with a solid is reached. Two distinct sets of solids have been considered in the calculations (Table 4-4).

The first set allows the precipitation of solid solutions involving either Ba or Ra. The more relevant solid solution is $(Ba,Ra)SO_4$, which is treated as ideal. In addition, dolomite and anhydrite have also been considered. The second set does not include solid solutions but pure phases (barite and $RaSO_4$(s), together with calcite, dolomite and anhydrite). The results obtained with both sets are compared to determine the solubility limit reduction caused by the precipitation of solid solutions. It is very important to bear in mind that sulphate is set constant in the calculations, because it is considered that sulphate from porewater quickly diffuses to the canister after sulphate minerals precipitate, maintaining a constant concentration.

Table 4-4. List of solid phases allowed to precipitate during the release of Ra and Ba from the spent fuel dissolution.

Set 1	Set 2
$(Ba,Ra)SO_4$ ideal solid solution	$RaSO_{4\,(c)}$
$(Ba,Ra)CO_3$ ideal solid solution	$BaSO_4$
$(Ba,Ca)CO_3$ regular solid solution, a = 6.7	$BaCO_3$
$(Ra,Ca)CO_3$ regular solid solution, a = 6.7	$CaCO_3$
$CaMg(CO_3)_2$	$CaMg(CO_3)_2$
$CaSO_4$	$CaSO_4$

Results

Solid solution calculations considering solid phases listed in *set 1* (Table 4-4) show that saturation in $(Ba,Ra)SO_4$ is quickly attained (15 years; Figure 4-9) asuming that the canister void volume is instananeously filled with 1,000 L, and at the considered dissolution rate. After saturation, barium and radium concentrations are fixed at 7.4×10^{-8} mol·L^{-1} and 2.0×10^{-11} mol·L^{-1}, respectively (Figure 4-9 and Figure 4-10).

Radium speciation is dominated by Ra^{2+} but with a concentration close to $RaSO_{4\ (aq)}$ (Table 4-5). The other species included in the calculations, $RaCl^+$, $Ra(OH)^+$ and $RaCO_3$ (aq), are much less concentrated. From this speciation, it can be concluded that at [Cl^-] as in the Forsmark groundwater, radium mobility is not influenced by chloride complex formation.

Table 4-5. Radium speciation in equilibrium with $(Ba_{0.99942}Ra_{0.00057})SO_4$ solid solution, which is the first solid to precipitate.

Species	Concentration (mol·L^{-1})
Ra^{2+}	1.17×10^{-11}
$RaSO_{4\ (aq)}$	1.06×10^{-11}
$RaCl^+$	3.54×10^{-13}
$RaCO_{3\ (aq)}$	5.55×10^{-16}
$RaOH^+$	9.76×10^{-19}

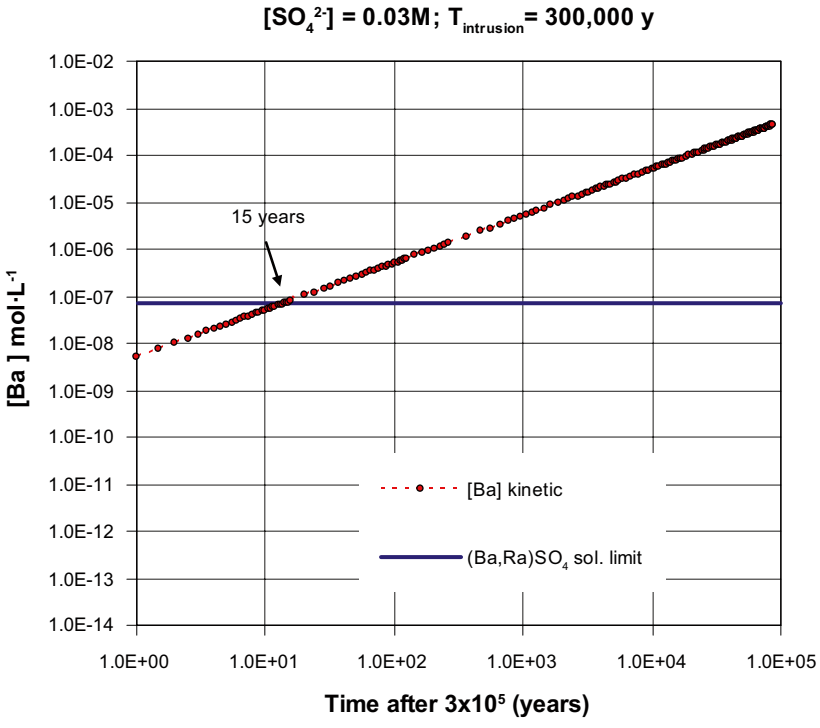

Figure 4-9. *Evolution of barium releases in the canister after instantaneous water intrusion in the conditions for the reference case ([SO_4^{2-}]=0.03 mol·L^{-1}). Intrusion occurs 300,000 years after spent fuel storage. The dotted red line indicates the calculated releases of Ba(II) without taking into consideration the precipitation of sulphate solid phases. However, saturation with respect to $(Ba,Ra)SO_4$ solid solution is quickly attained (15 years), and barium concentration in solution is kept at 7.4×10^{-8} mol·L^{-1}.*

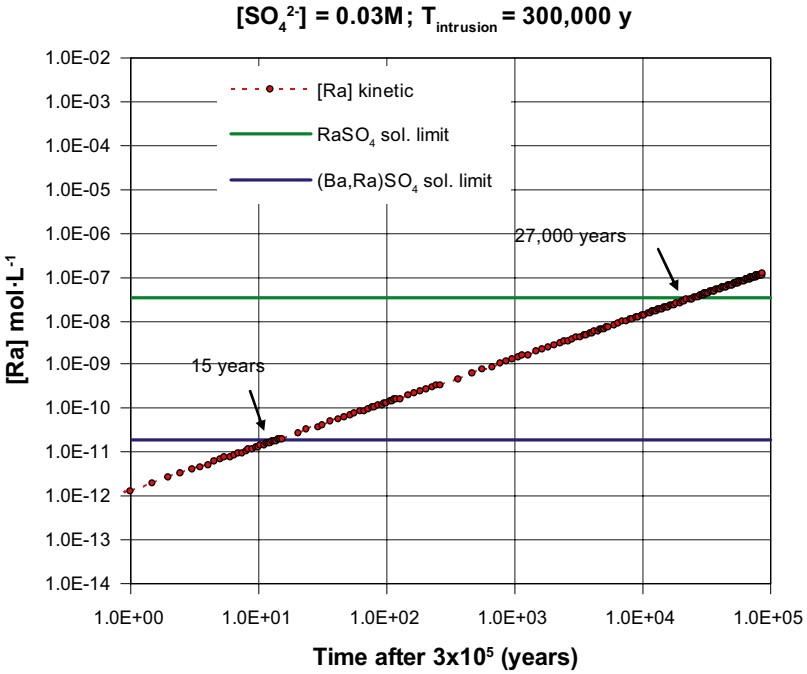

Figure 4-10. *Evolution of radium releases in the canister after instantaneous water intrusion in the conditions of the reference case ($[SO_4^{2-}]$ = 0.03 mol·L^{-1}). Intrusion occurs 300,000 years after spent fuel storage. The red dotted line indicates the calculated Ra(II) releases assuming no precipitation of sulphate phases. However, saturation with respect to (Ba,Ra)SO_4 solid solution is quickly attained (15 years), while $RaSO_4$ (s) would start to precipitate after 27,500 years. The calculated dissolved radium concentration in equilibrium with the solid solution is 2.0×10^{-11} mol·L^{-1}, which is much lower than in the case of equilibrium with the pure phase ($[Ra_{tot}] = 3.5\times10^{-8}$ mol·L^{-1}).*

The composition of the first solid solution in equilibrium with the intruding groundwater is $(Ba_{0.99942}Ra_{0.00057})SO_4$. With this composition the ideal approach is reinforced (see the discussion in previous sections). No other solid solution involving radium precipitates.

If the reference solution dissolving the spent fuel is equilibrated with the solid phases listed in *set 2* (Table 4-4), radium solubility is controlled by $RaSO_4$ (s), yielding $[Ra_{total}] = 3.5\times10^{-8}$ mol·L^{-1}, 3 orders of magnitude higher than in the case of solid solution equilibrium. Barium concentration in equilibrium with pure barite is almost identical to that in the solid solution case, since the solid solution calculated above has a composition very close to pure barite ($X_{barite\ (molar)} = 0.99942$).

Sensitivity analysis: the effect of sulphate concentration

As reported in Section 4.3, sulphate concentration in porewater may undergo sudden changes, affecting the formation of (Ba,Ra)SO_4 solid solution. As a sensitivity analysis, three additional sulphate concentrations have been tested: 0.3 mol·L^{-1}, 0.003 mol·L^{-1} and 0.0003 mol·L^{-1}. Results are shown in Figure 4-11. Considering a sulphate concentration of 0.3 mol·L^{-1}, the solubility limit for radium is lower than in the reference case since the saturation with a solid solution is attained faster and radium dissolved during this time is smaller. In contrast, the solubility limit is progressively higher as sulphate concentration decreases, since more radium has been dissolved in the fuel until saturation in a (Ba,Ra)SO_4 solid solution. The solubility limit of radium is not linear in Figure 4-9 due to the effect of the increased ionic strength on the divalent ion activities. The expected radium concentration at the lowest sulphate content is relatively high (7.3×10^{-10} mol·L^{-1}), although it is more than three orders of magnitude lower than the limit calculated by assuming equilibrium with the pure phases ($[Ra_{total}]=1.3\times10^{-6}$ mol·L^{-1}).

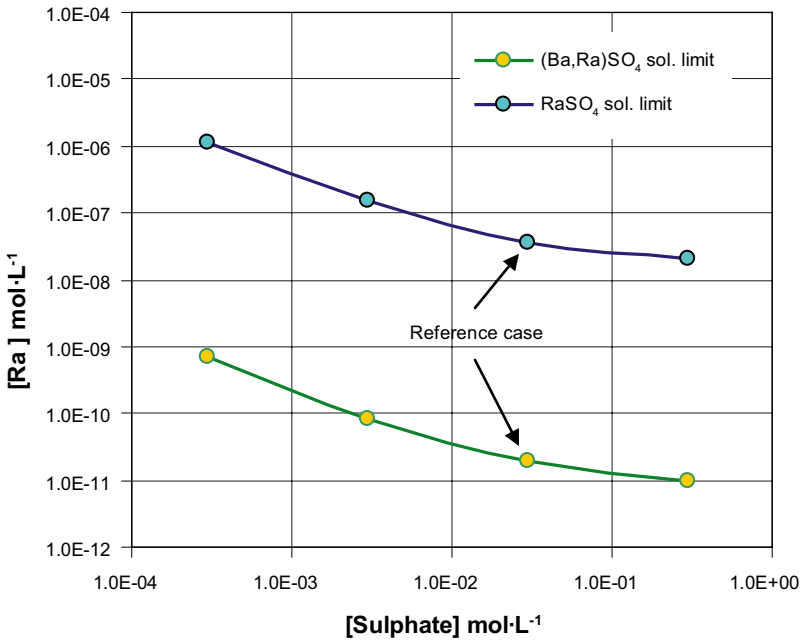

Figure 4-11. *Radium solubility limit as a function of total sulphate concentration in the canister after water intrusion. Different sulphate concentrations in the intruding groundwater have been considered (0.0003, 0.003, 0.03 and 0.3 mol·L^{-1}). Intrusion occurs 300,000 years after spent fuel storage.*

4.5 The kinetics of Ra(II) incorporation into an existing $BaSO_4$(s)

The main thermodynamic constraints concerning the stability of $RaBaSO_4$(ss) have been thoroughly discussed. It is quite clear that in the case that Ra and Ba are released contemporaneously in the expected ratios from spent fuel, they will coprecipitate and build stable solid solutions. However, it remains to be discussed to which extent this is applicable to the secondary release of ^{226}Ra from UO_2(s) that has precipitated away from the fuel. What follows is an attempt to rationalise this scenario.

There are no specific experimental studies on the mechanisms and rates of incorporation of Ra(II) into the Ba(II) sulphate structure. Most of the experimental and theoretical studies have been devoted to the growth mechanisms of barite /Pina et al. 1998, Dunn et al. 1999, Risthaus et al. 2001/ and the growth of celestite ($SrSO_4$(s)) onto the barite structure /Pina et al. 2004, Sanchez-Pastor et al. 2005, 2006ab/.

The growth mechanism of barite is quite dependent on the state of saturation with respect to the solid phase. For close to saturation conditions the mechanism of growth is monodimensional and rather slow, while for oversaturation conditions the mechanism is bidimensional and relatively fast. The growth of celestite onto the barite structure requires substantial oversaturation and this has been explained in terms of the major lattice structure difference between the two sulphate phases.

In their seminal work /Doerner and Hoskins 1925/ made a careful experimental study of the surface precipitation (they called *replacement*) of Ra(II) onto $BaSO_4$(s) from which they derived their logarithmic distribution law. Their experiments were made by adding a known $RaCl_2$ solution to a Ba(II) sulphate precipitate. The experiments were performed in acid media with a total acidity ranging between 0.0053 and 0.185 mol·L^{-1} HCl and the experimental conditions were varied in order to establish the relationship between the observed Ra(II) partition and a number of experimental parameters. For instance the amount of initial $BaSO_4$(s) was varied as well as the digestion time and temperature of the resulting solid phase. The main outcome

of their experimental study of the *replacement* process was that the solid phase did not reach equilibrium in five days, in spite of the various digestion techniques used and more importantly that the overall rate and extent of the *replacement* process was very much dependent on the crystal growth effects of the precipitated Ba(II) sulphate. They also indicated that temperature and acidity had a profound effect on crystal growth and stated that when the contact between the $RaCl_2$ solution and the $BaSO_4$ solid phase was made in neutral conditions and in cold conditions, no measurable uptake of Ra(II) was observed in four contact days. This evidence prompted the authors to state that adsorption was not the process responsible for the measured uptake under more dynamic conditions for the existing solid phase.

A completely different behaviour was observed by the authors when the experiments were performed under the *coprecipitation* mode, this is by adding sulphuric acid to an existing Ra(II), Ba(II) chloride solution. In this case, equilibrium was reached between the aqueous and the solid phases and a normal distribution law could be used to describe the equilibrium condition.

The only known published study on the sorption of Ra(II) onto barite and pure $BaSO_4$(s) is by /Wang et al. 1993/. This experimental study is devoted to determining the extent of adsorption of Ra(II) on different mineral surfaces including Ba(II) sulphates. The authors performed static and dynamic (column) studies and established that in the static experiments up to 86.7% of the initial radium was adsorbed on $BaSO_4$(s) in 24 hours of contact with a solution at pH=7.8 and at 18°C. The degree of adsorption was 81.6% in natural barite which contained up to 9.6% of SiO_2.

In the dynamic experiments the adsorption of Ra(II) onto barite was quantitative (99.5%) after 10,000 bed volumes of the 5,037 pCi L^{-1} Ra(II) solution have been percolated through.

In spite of these very efficient results, no attempt was made by the authors to explore the actual retention mechanism although they pointed out the possibility of a cation exchange mechanism between Ba(II) and Ra(II) to explain the sorption data.

Hence, even if all the direct and indirect evidence points out towards a fast incorporation of Ra(II) onto an existing Ba(II) sulphate structure, there is a need to perform a devoted mechanistic study to fully back up the macroscopic findings. Currently, such an experimental investigation is underway in collaboration with the Institute for Nuclear Safety of the Karlsruhe Research Center.

5 Conclusions

Radium incorporation into (Ba,Ra)SO_4 solid solutions is a well-known process which controls the solubility of ^{226}Ra in most natural and anthropogenic waters. (Ba,Ra)SO_4 solid solutions are ubiquitous precipitates in industrial and mining activities.

The structural and thermodynamic properties of the resulting solid solution have been thoroughly studied and the aqueous solution/solid solution equilibria can be properly described by well known thermodynamic principles.

Calculations using an ATM-104 fuel at 40 MWd/kg U show that barium and radium inventories per canister progressively grow with time after deposition. Most of the barium is produced in the initial 500 years. In the unlikely event of a contact of sulphate-containing groundwaters with the fuel, Ba(II) will precipitate as $BaSO_4$(s). The production of ^{226}Ra reaches its peak some 300,000 years after deposition. This substantial time gap indicates that most of the $BaSO_4$(s) will be present when and if radium is released from the fuel, even if some Ra and Ba will be released contemporaneously.

Two potential scenarios have been addressed from the mechanistic point of view. In the event of a simultaneous release of Ra with Ba, the former will be readily incorporated into the precipitating $BaSO_4$ to build a Ra Ba sulphate solid solution. All the existing evidence indicates, that in this case, the behaviour of the system can be described by the established aqueous-solid solution thermodynamic formalism and assuming that the system behaves ideally. In the case when ^{226}Ra is released from a secondary source, like a UO_2 precipitate away from the fuel but within the canister, there is not sufficient experimental information at the molecular level to establish when and how the system will reach equilibrium and, therefore, it is not clear to which extent the aqueous-solid solution thermodynamic formalism can be applied. Nevertheless, the long contact times expected under repository conditions together with the small mass transfer processes involved would indicate that it is quite likely that equilibrium will be reached. Dedicated experimental investigations are under way in collaboration with INE-KFZ to establish the mechanism and rates of this critical process in order to support the solid solution thermodynamic approximation.

We have performed a number of scoping calculations in order to establish the absolute and relative effects of $RaBaSO_4$(ss) formation on ^{226}Ra solubility. We have assumed that the free volume per canister filled by water in case of intrusion is roughly 1 m^3. By using the standard fuel dissolution rate of 1.0×10^{-7} y^{-1}, and a congruent release of barium, the calculated radium and barium concentrations after one year of contact at the disposal time of 300,000 years (when the ^{226}Ra content is largest), are 1.3×10^{-12} and 4.9×10^{-9} mol·L^{-1}, respectively. If we apply the thermodynamics of aqueous-solid solution equilibria the resulting solid phase in equilibrium has a calculated nominal composition of $(Ba_{0.99942}Ra_{0.00057})SO_4$ (ss) and the resulting dissolved Ra(II) is in the 10^{-11} mol L^{-1} range. This is in the upper range of any observed Ra(II) concentration in natural and anthropogenic environment. If the solubility of Ra(II) is assumed to be controlled by the precipitation of a pure sulphate phase, the resulting concentration is three orders of magnitude higher. A concentration never observed in natural systems.

Since sulphate concentration can be highly variable due to changes in the nature of the groundwaters flowing into the near field, we have performed a sensitivity study of the influence of the sulphate concentrations in the expected concentration range. In the case when the lowest concentration is assumed ($[SO_4^{2-}]= 3\times10^{-4}$ mol·L^{-1}), the calculated radium solubility increases up to 7.1×10^{-10} mol·L^{-1} when equilibrium with the solid solution is considered. The calculated individual solubility of $RaSO_4$(s) under these conditions is and 1.13×10^{-6} mol·L^{-1}.

6 Acknowledgements

The content and shape of the text have been greatly improved by the review comments of Virginia Oversby, Patrik Sellin and Kastriot Spahiu.

7 References

Al-Masri M S, Suman H, 2003. NORM waste management in the oil and gas industry: The Syrian experience. *Journal of Radioanalytical and Nuclear Chemistry*, 256, 159–162.

Amber, 2006. Amber 5 Reference Guide. Version 1.0, December 2006. Enviros Consulting Limited. www.enviros.com/amber.

Andrews J N, Ford D J, Hussain N, Trivedi D, Youngman M J, 1989. Natural radioelement solution by circulating ground waters in the Stripa granite. *Geochimica et Cosmochimica Acta* 53, 1791–1802.

Arcos D, Grandia F, Domènech C, 2006. Geochemical evolution of the near field of a KBS-3 repository. SKB TR-06-16, Svensk Kärnbränslehantering AB.

Beaucaire C, Criaud A, Michard G, 1987. Contrôle des concentrations de certains éléments traces (As, Sb, U, Ra, Ba) dans les eaux du Cézallier (Massif Central, France). *Chemical Geology*, 63, 85–99.

Beddow H, Black S, Read D, 2006. Naturally occurring radioactive material (NORM) from a former phosphoric acid processing plant. *Journal of Environmental Radioactivity*, 86, 289–312.

Benes P, 1984. Migration of radium in the terrestrial hydrosphere in the behaviour of radium in waterways and aquifers. IAEA Rep., IAEA-TECDOC-301, 119.

Berner U, Curti E, 2002. Radium solubilities from SF/HLW wastes using solid solution and co-precipitation models, Paul Scherrer Institute, Villigen, Switzerland, Internal Report TM-44-02-04.

Blount C W, 1977. Barite solubilities and thermodynamic quantities up to 300°C and 1,400 bars. *American Mineralogist,* 62, 942–957.

Boström K, Frazer J, Blankenburg J, 1967. Subsolidus phase relations and lattice constants in the system $BaSO_4$-$SrSO_4$-$PbSO_4$. *Ark. Mineral. Geol.*, 4, 447–485.

Bruno J, Bosbach D, Kulik D, Navrotsky A, 2007. Chemical Thermodynamics of Solid Solutions of Interest in Radioactive Waste. *Chemical Thermodynamics Series*. NEA.

Burnett W C, Elzerman A W, 2001. Nuclide migration and the environmental radiochemistry of Florida phosphogypsum. *Journal of Environmental Radioactivity,* 54, 27–51.

Ceccarello S, Black S, Read D, Hodson M E, 2004. Industrial radioactive barite scale: suppression of radium uptake by introduction of competing ion, *Miner. Eng.,* 17, 323–330.

Chang L L Y, Howie R A, Zussman J, 1996. *Non-silicates: Sulfates, carbonates, phosphates, halides*. Rock-forming minerals vol. 5B, 383 pp.

Church T M, 1970. Marine barite. *Ph. D. Thesis,* University of California San Diego.

Cramer J, Smellie J (eds), 1994. Final Report of the AECL/SKB Cigar Lake Analog Study. SKB TR 94–04, Svensk Kärnbränslehantering AB.

Curie M P, Curie Mme P, Bémont M G, 1898. On a new, strongly radioactive substance, contained in pitchblende. *Comptes Rendus* 127, 1215–7.

Curie M P, 1911. Radium and the New Concepts in Chemistry. *Nobel Prize Lecture*

Doerner H, Hoskins W M, 1925. Co-precipitation of barium and radium sulphates. *J. Am. Chem. Soc.*, 47, 662–675.

Dunn K, Daniel E, Shuler P J, Chen H J, Yongchun T, Yen T F, 1999. Mechanisms of surface precipitation and dissolution of barite. A morphology approach. *J. Colloid and Interface Sci. 427–437.*

Duro L, Grivé M, Cera E, Gaona X, Domènech C, Bruno J, 2006. Determination and assessment of the concentration limits to be used in SR-Can. SKB TR-06-32, Svensk Kärnbränslehantering AB.

Fedorak P M, Westlake D W S, Anders C, Kratochvil B, Motkosky N, Anderson W B, Huck P M, 1986. Microbial release of Ra-226 from (Ba,Ra)SO_4 sludges from uranium mine wastes. *Appl. Environ. Microbiol.*, 52, 262–268.

Felmy A R, Rai D, Moore D A, 1993. The solubility of (Ba,Sr)SO_4 precipitates: thermodynamic equilibrium and reaction path analysis. *Geochimica et Cosmochimica. Acta*, 57, 4345–4363.

Fisher R S, 1998. Geologic and geochemical controls on Naturally Occurring Radioactive Materials (NORM) in produced water from oil, gas and geothermal operations. *Environmental Geoscience*, 5-3, 139–150.

Foster D A, Staubwasser M, Henderson G M, 2004. ^{226}Ra and Ba concentrations in the Ross Sea measured with multicollector ICP mass spectrometry. *Marine Chemistry*, 87, 59– 71.

Gamsjäger H, Königsberger E, Preis W, 2000. Lippmann diagrams: theory and application to carbonate systems. *Aquatic Geochemistry*, 6, 119– 132.

Germann F E E, 1921. Adsorption of radium by barium sulphate. *J. Amer. chem. Soc.*, 43, 1615–1621.

Glynn P D, 1990. Modeling solid-solution reactions in low temperature aqueous systems. In: Bassett, R. L. and Melchior, D. C., (Eds.), Chemical modeling in aqueous systems II, *American Chemical Society* 416, 74–86.

Glynn P D, Reardon E J, 1990. Solid-solution aqueous-solution equilibria: thermodynamic theory and representation. *American Journal of Science,* 290, 164–201.

Glynn P D, Reardon E J, Plummer L N, Busenberg E, 1990. Reaction paths and equilibrium end-points in solid-solution aqueous-solution systems. *Geochimica et Cosmochimica Acta*, 54, 267–282.

Glynn P D, 1991. MBSSAS: a computer code for the computation of Margules parameters and equilibrium relations in binary solid-solution aqueous-solution systems. *Comput. Geosci.*,17, 907–966.

Glynn P D, 2000. Solid solution solubilities and thermodynamics: Sulfates, carbonates and halides, In: Jambor, J.L., Nordstrom, D.K. (Eds.), *Sulfate Minerals: Crystallography, Geochemistry and Environmental Significance*. Reviews in Mineralogy and Geochemistry, 40, Mineralogical Society of America and Geochemical Society, Washington, D.C., 481–511.

Goldschmidt B, 1938. Sur la précipitation mixte des sulfates de baryum et strontium. *C. R. Hebd. Séances Acad. Sci.*, 206, 1110.

Gordon L, Rowley K, 1957. Coprecipitation of radium with barium sulphate. *Anal. Chem*., 29, 34–37.

Grahmann W, 1920. Uber barytocolestin und das verhaltnis von anhydrit zu colestin und baryt. *Neues Jahrb. Mineral*., 1, 1–23.

Grundl T, Cape M, 2006. Geochemical factors controlling radium activity in a sandstone aquifer. *Ground Water*, 44-4, 518–527.

Guggenheim E A, 1937. Theoretical basis of Raoult's law. *Trans. Faraday Soc.*, 33, 151–159.

Hamlat M S, Kadi H, Fellag H, 2003. Precipitate containing norm in the oil industry: modelling and laboratory experiments. *Applied Radiation and Isotopes,* 59, 95–99.

Hanor J S, 1968. Frequency distribution of compositions in the barite-celestite series. *American Mineralogist*, 53, 1215–1222.

Hanor J S, 2000. Barite-celestite geochemistry and environments of formation. In: Jambor, J.L., Nordstrom, D.K. (Eds.), *Sulfate Minerals: Crystallography, Geochemistry and Environmental Significance*. Reviews in Mineralogy and Geochemistry, 40, Mineralogical Society of America and Geochemical Society, Washington, D.C., 193–275.

Hawthorne F C, Krivovichev S V, Burns P C, 2000. The crystal chemistry of sulfate minerals. In: Jambor, J.L., Nordstrom, D.K. (Eds.), *Sulfate Minerals: Crystallography, Geochemistry and Environmental Significance*. Reviews in Mineralogy and Geochemistry, 40, Mineralogical Society of America and Geochemical Society, Washington, D.C., 1–112.

Huck P M, McClymont G L, Schwartz F W, Nesbitt B E, Anderson W B, Kratochvil B, 1989. Modelling of radium-226 leaching from radium-barium sulfate sludges. *Waste Management*, 9, 157–163.

Håkansson R, 1999. Beräkning av nuklidinnehåll, resteffekt, aktivitet samt doshastighet för utbränt kärnbränsle. SKB R-99-74, Svensk Kärnbränslehantering AB.

Jerez-Vegueria S F, Godoy J M, Miekeley N, 2002. Environmental impact studies of barium and radium discharges by produced waters from the "Bacia de Campos" oil-field offshore platforms, Brazil. *Journal of Environmental Radioactivity*, 62, 29–38.

Knett J, 1904. Indirekter Nachweis von Radium in den Karlsbader Thermen–Sitzungsber. *Akad. Wis. Wien*, 113, Abt. II.a, 753–762.

Kornicker W A, Presta P A, Paige C R, Johnson D M, Hileman O E, Snodgrass W J, 1991. The aqueous dissolution kinetics of the barium/lead sulphate solid solution series at 25°C and 60°C. *Geochimica et Cosmochimica Acta*, 55, 3531–3541.

Kraemer T F, Reid D F, 1984. The occurrence and behavior of radium in saline formation water of the US Gulf Coast region. *Chemical Geology (Isotope Geoscience)*, 2, 153–174.

Kulik D A, Kersten M, Heiser U, Neumann T, 2000. Application of Gibbs energy minimization to model early-diagenetic solid-solution aqueous-solution equilibria involving authigenic rhodochrosites in anoxic Baltic Sea sediments. *Aquatic Geochemistry*, 6,147–199.

Kulik D, Berner U, Curti E, 2004. Modelling chemical equilibrium partitioning with the GEMS-PSI code. In: Smith, B., Gschwend, B. (Eds.), PSI Scientific Report 2003/Volume IV. Nuclear Energy and Safety, Paul Scherrer Institute, Villigen, 109–122.

Kulik D A, 2006. Dual-thermodynamic estimation of stoichiometry and stability of solid solution end members in aqueous–solid solution systems. *Chemical Geology*, 225,189–212.

Langmuir D, Melchior D, 1985. The geochemistry of Ca, Sr, Ba and Ra sulfates in some deep brines from the Palo Duro Basin, Texas. *Geochimica et Cosmochimica Acta*, 49, 2423–2432.

Langmuir D, Riese A C, 1985. The thermodynamic properties of radium. *Geochimica et Cosmochimica Acta*, 49, 1593–1601.

Lee J S, Wang H R, Izuka Y, Yu S C, 2005. Crystal structure and Raman spectral studies of $BaSO_4$-$PbSO_4$ solid solution, *Z. Kristallogr*., 220, 1–9.

Lippmann F, 1977. The solubility products of complex minerals, mixed crystals, and three-layer clay minerals. *Neues Jahrb. Mineral. Abh.,* 130, 243–263.

Lippmann F, 1980. Phase diagrams depicting aqueous solubility of binary mineral systems. *Neues Jahrb. Mineral. Abh.,* 139, 1–25.

Lippmann F, 1982. Stable and metastable solubility diagrams for the system $CaCO_3$-$MgCO_3$-H_2O at ordinary temperatures. *Bull. Mineral.*, 105, 273–279.

Marques B E, 1936. The fractionation of barium salts containing radium. *Journal de Chimie Physique et de Physico-Chimie Biologique*, 33, 1–40.

Martin P, Akber R A, 1999. Radium isotopes as indicators of adsorption-desorption interactions and barite formation in ground water. *Journal of Environmental Radioactivity*, 46, 271–286.

Martin A J, Crusius J, McNee J J, Yanful E K, 2003. The mobility of radium-226 and trace metals in pre-oxidized subaqueous uranium mill tailings. *Applied Geochemistry*, 18, 1095–1110.

McCready R G L, Bland C J, Gonzales D E, 1980. Preliminary studies on the chemical, physical and biological stability of Ba/$RaSO_4$ precipitates. *Hydrometallurgy,* 5,109–116.

McKenzie A B, Scott R D, Linsalata P, Miekeley N, 1993. Natural decay series studies of the redox front system in the Poços de Caldas uranium mineralisation. *J. of Geochem. Explor.* 45 (1–3), 289–322.

Moise T, Starinsky A, Katz A, Kolodny Y, 2000. Ra isotopes and Rn in brines and ground waters of the Jordan-Dead Sea Rift Valley: Enrichment, retardation, and mixing. *Geochimica et Cosmochimica Acta*, 64-14, 2371–2388.

Momoshima N, Nita J, Maeda Y, Sugihara S, Shinno I, Matsuoka N, Huang C W, 1997. Chemical Composition and Radioactivity in Hokutolite (Plumbian Barite) Collected at Peito Hot Spring, Taiwan. *Journal of Environmental Radioactivit*y, 37-1, 85–99.

Moore W S, 1997. High fluxes of radium and barium from the mouth of the Ganges-Brahmaputra River during low river discharge suggest a large groundwater source. *Earth and Planetary Science Letters*, 150, 141–150.

Motamedi M, Karnland O, Pedersen K, 1996. Survival of sulphate reducing bacteria at different water activites in compacted bentonite. *FEMS Microbiology Letters*, 141, 83–87.

Nikitin B, Tolmatscheff P, 1933. Ein beitrag zur gultigkeit der massen wirkungsgesetzes. II. Quantitative bestimmung der loslichkeit radiumsulfates in natriumsulfatlosungen und in wasser. *Z. Phys. Chem.*, A167, 260.

Nordstrom D K, Ball J W, Donahoe R J, Whittemore D, 1989. Groundwater chemistry and water-rock interactions at Stripa. *Geochimica et Cosmochimica Acta* 53, 1727–1740.

Nozaki Y, Yamamoto Y, Manaka T, Amakawa H, Snidvongs A, 2001. Dissolved barium and radium isotopes in the Chao Phraya River estuarine mixing zone in Thailand. *Continental Shelf Research* 21, 1435–1448.

Paridaens J, Vanmarcke H, 2001. Radium contamination of the banks of the river Laak as a consequence of the phosphate industry in Belgium. *Journal of Environmental Radioactivity*, 54, 53–60.

Phillips E J, Landa E R, Kraemer T, Zielinsky R, 2001. Sulfate-reducing bacteria releases barium and radium from naturally occurring radioactive material in oil-field barite. *Geomicrobiology Journal*, 18-2, 167–182.

Pina C M, Becker U, Risthaus P, Bosbach D, Putnis A, 1998. Molecular scale mechanisms of crystal growth in barite. *Nature, 395* 483–488.

Pina C M, Putnis A, Astilleros J M, 2004. The growth mechanisms of solid solutions crystallising from aqueous solutions. *Chemical Geology*, 204, 145–161.

PNL, 1991. Characterization of Spent Fuel Approved Testing Material – ATM-104. Pacific Northwest Laboratory Report, 1991, PNL-5109-104/UC-802.

Prieto M, Fernández-González A, Putnis A, Fernández-Díaz L, 1997. Nucleation, growth, and zoning phenomena in cristallizing (Ba,Sr)CO_3, Ba(SO_4,CrO_4), (Ba,Sr)SO_4, and (Cd,Ca)CO_3 solid solutions from aqueous solutions. *Geochimica et Cosmochimica Acta*, 61, 3383–3397.

Prieto M, Fernández-González A, Becker U, Putnis A, 2000. Computing Lippmann diagrams from direct calculation of mixing properties of solid solutions: Application to the barite-celestite system. *Aquatic Geochemistry*, 6, 133–146.

Redlich O, Kister A T, 1948. Algebraic representation of thermodynamic properties and the classification of solutions. *Ind. Eng. Chem.*, 40-2, 345–348.

Rihs S, Condomines M, Sigmarsson O, 2000. U, Ra and Ba incorporation during precipitation of hydrothermal carbonates: Implications for ^{226}Ra-Ba dating of impure travertines. *Geochimica et Cosmochimica Acta*, 64, 661–671.

Risthaus P, Bosbach D, Becker U, Putnis A, 2001. Barite scale formation and dissolution at high ionic strength studied witj atomic force microscopy. *Colloid and Surfaces A, 191* 201–214.

Romero L, Thompson A, Moreno L, Neretnieks I, Widén H, Boghammar A, 1999. Comp23/ Nuctran user´s guide – Proper version 1.1.6. SKB R-99-64, Svensk Kärnbränslehantering AB.

Rutherford P M, Dudas M J, Arocena J M, 1996. Heterogeneous distribution of radionuclides, barium and strontium in phospogypsum by product, *Sci. Total Environ.*, 180, 201–209.

Sanchez-Pastor N, Pina C M, Astilleros J M, Fernandez-Diaz L, Putnis A, 2005. Epitaxial growth of celestite on barite (001) face at a molecular scale. *Surface Sci*. 225–235.

Sanchez-Pastor N, Pina C M, Astilleros J M, Fernandez-Diaz L, 2006a. Relationships between cristal morphology and composition in the (Ba, Sr)SO_4–H_2O solid solution-aqueous solution system. *Chemical Geology* 266–277.

Sanchez-Pastor N, Pina C M, Astilleros J M, Fernandez-Diaz L, 2006b. The effect of CO_3^{2-} on the growth of barite {001} and {210} surfaces: An AMF study. *Surface Sci.* 1369–1381.

Sebesta F, Benes P, Sedlacek J, John J, Sandrik R, 1981. Behavior of radium and barium in a system including uranium mine waste waters and adjacent surface waters. American Chemical Society, 15-1, 71–75.

SKB, 2006a. Long-term safety for KBS-3 repositories at Forsmark an Laxemar – a first evaluation Main Report of the SR-Can project. SKB TR-06-09, Svensk Kärnbränslehantering AB.

SKB, 2006b. Data report for the safety assessment SR-Can. SKB TR-06-25, Svensk Kärnbränslehantering AB.

SKB, 2006c. Model summary report for the safety assessment SR-Can. SKB TR-06-26, Svensk Kärnbränslehantering AB.

Smith A L, 1987. Radioactive-scale formation. *Journal of Petroleum Technology* (June), 697–706.

Snodgrass W J, Hileman O E, 1985. On the geochemical mechanism controlling Ra-226 dissolution in uranium mill wastes (tailings). Uranium Tailings Program, Energy Mines and Resources, Government of Canada.

Sorbie K S, Mackay E J, 2000. Mixing of injected, connate and aquifer brines in waterflooding and its relevance to oilfield scaling. *Journal of Petroleum Science and Engineering*, 27, 1-2, 85–106.

Starke R, 1964. Die strontiumgehälte der baryte. *Freiberg. Forschungsh C.*, 150, 123.

Struebel G, 1966. Die hydrothermale löslichkeit von cölestin in system $SrSO_4$–NaCl–H_2O. *Neues Jahrb. Mineral. Mon.*, 99–107.

Sturchio N, Bohlke J, Markun F, 1993. Radium geochemistry of geothermal waters, Yellowstone National Park, Wyoming, USA. *Geochimica et Cosmochimica Acta,* 57-6, 1203–1214.

Sturchio N, Banner J, Binz C, Heraty L, Musgrove M, 2001. Radium geochemistry of ground waters in Paleozoic carbonate aquifers, mid-continent, USA. *Applied Geochemistry* 16, 109–122.

Takano B, Yanagisawa M, Watanuki K, 1969. Structure gap in $BaSO_4$–$PbSO_4$ solid solution series, *Mineral. J.,* 6, 159–171.

Wang H R, Lee J S, Yu S C, 2002. Synthesis of zoning-free $BaSO_4$–$PbSO_4$ solid solutions and its structural characterizations. *Z. Kristallogr.*, 217, 143–148.

Wang R S, Chau A S Y, Liu F, Cheng H, Nar P, Chen X M, Wu Q Y, 1993. Studies on the adsorption and migration of radium in natural minerals. J. Radioanal.and Nuc. Chem. 171, 347–364.

Werme L O, Johnson L H, Oversby V M, King F, Spahiu K, Grambow B, Shoesmith D W, 2004. Spent fuel performance under repository conditions: A model for use in SR-Can. SKB TR-04-19, Svensk Kärnbränslehantering AB.

Wilson W F, 1994. A guide to naturally occurring radioactive material. PennWell Publishers, Tulsa, OK.

YuHang C, Asenjo A, Sánchez-Pastor N, Fernández-Díaz L, Gómez J, Pina C M, 2007. Growth of $Ba_xSr_{1-x}SO_4$ nano-steps on barite (001) face. *Surface Science*, 601, 381–389.

Zhu C, 2004a. Coprecipitation in the barite isostructural family:1. Binary mixing properties. *Geochimica et Cosmochimica Acta*, 68, 3327–3337.

Zhu C, 2004b. Coprecipitation in the barite isostructural family:2. Numerical simulations of reactions and mass transport. *Geochimica et Cosmochimica Acta*, 68, 3339–3349.

Zukin J G, Hammond D E, Ku T-L, Elders W A, 1987. Uranium-thorium series isotopes in brines and reservoir rocks from two deep geothermal well holes in the Salton Sea geothermal field, southeastern California. *Geochimica et Cosmochimica Acta*, 31, 2719–2731.

Appendix A

Aqueous-solid solution equilibrium: The Lippmann's concepts

The equilibrium between an aqueous electrolyte and a mixed ionic solid, e.g. (Ba,Ra)SO_4, can be expressed by two law-of-mass action (LMA) Equations A-1 and A-2:

$$\{Ba^{2+}\}\{SO_4{}^{2-}\} = K_{BaSO_4} a_{BaSO_4} = K_{BaSO_4} x_{BaSO_4} f_{BaSO_4} \quad \text{(Equation A-1)}$$

$$\{Ra^{2+}\}\{SO_4{}^{2-}\} = K_{RaSO_4} a_{RaSO_4} = K_{RaSO_4} x_{RaSO_4} f_{RaSO_4} \quad \text{(Equation A-2)}$$

where $\{SO_4{}^{2-}\}, \{Ba^{2+}\}, \{Ra^{2+}\}$ are the aqueous activities of $SO_4{}^{2-}$, Ba^{2+}, Ra^{2+}; K_{BaSO_4} and K_{RaSO_4} are the solubility products of pure $BaSO_4$ and $RaSO_4$ end members with activities a_{BaSO_4}, a_{RaSO_4}, mole fractions x_{BaSO_4}, x_{RaSO_4}, and activity coefficients f_{BaSO_4}, f_{RaSO_4}, respectively.

As above mentioned, /Lippmann 1977, 1980, 1982/ introduced the *total solubility product ΣΠ* defined as (for the Ra-Ba-SO_4 system, Equation A-3):

$$\Sigma\Pi_{eq} = \{SO_4{}^{2-}\} \cdot \left(\{Ba^{2+}\} + \{Ra^{2+}\}\right) \quad \text{(Equation A-3)}$$

From this equation, a curve called *solidus* can be drawn (Figure A-1), which allows the determination of the composition of a solid in a solid solution series. The equilibrium of the system is fully described if the total solubility product is expressed as a function of the aqueous composition. By applying Equation A-4, a curve called *solutus* is drawn (Figure A-1).

$$\Sigma\Pi_{eq} = 1 \Bigg/ \left(\frac{x_{Ba^{2+},aq}}{K_{Barite} f_{Barite}} + \frac{x_{RaSO_4,aq}}{K_{RaSO_4} f_{RaSO_4}} \right) \quad \text{(Equation A-4)}$$

where $X_{Ba^{2+},aq}$ and $X_{Ra^{2+},aq}$ are the aqueous activity fractions of Ba^{2+} and Ra^{2+} respectively. These mole fractions are defined in Equations A-5 and A-6:

$$x_{Ba^{2+},aq} = \frac{\{Ba^{2+}\}}{\{Ba^{2+}\} + \{Ra^{2+}\}}; \quad x_{Ra^{2+},aq} = \frac{\{Ra^{2+}\}}{\{Ba^{2+}\} + \{Ra^{2+}\}} \quad \text{(Equations A-5 and A-6)}$$

If a SS series is considered as ***ideal*** then the solid-phase activity coefficients f_{BaSO_4}, f_{RaSO_4}, are set to 1. However, in many natural solid solution systems, these coefficients depend on the composition of the equilibrium solid phase, showing a ***non-ideal*** behaviour. /Redlich and Kister 1948/ revealed that this dependence can be successfully described by using Equations A-7 and A-8, which in turn were derived from Equation A-9 suggested by /Guggenheim 1937/:

$$\ln f_{BaSO_4} = x_{RaSO_4}^2 \left[a_0 - a_1 \left(3x_{BaSO_4} - x_{RaSO_4}\right) + a_2 \left(x_{BaSO_4} - x_{RaSO_4}\right)\left(5x_{BaSO_4} - x_{RaSO_4}\right) + \ldots \right] \quad \text{(Equation A-7)}$$

$$\ln f_{RaSO_4} = x_{BaSO_4}^2 \left[a_0 + a_1 \left(3x_{RaSO_4} - x_{BaSO_4}\right) + a_2 \left(x_{RaSO_4} - x_{BaSO_4}\right)\left(5x_{RaSO_4} - x_{BaSO_4}\right) + \ldots \right] \quad \text{(Equation A-8)}$$

$$G^E = x_{RaSO_4} x_{BaSO_4} RT \left[a_0 + a_1 \left(x_{RaSO_4} - x_{BaSO_4}\right) + a_2 \left(x_{RaSO_4} - x_{BaSO_4}\right)^2 + \ldots \right] \quad \text{(Equation A-9)}$$

The latter equation shows the dependence of the excess free energy of the binary mixture as a function of solid solution composition. In general, such a dependence is well represented by using the first two terms (a_0 and a_1). There is an special case of non-ideality called ***regular system***, in which $a_0 = a_1$.

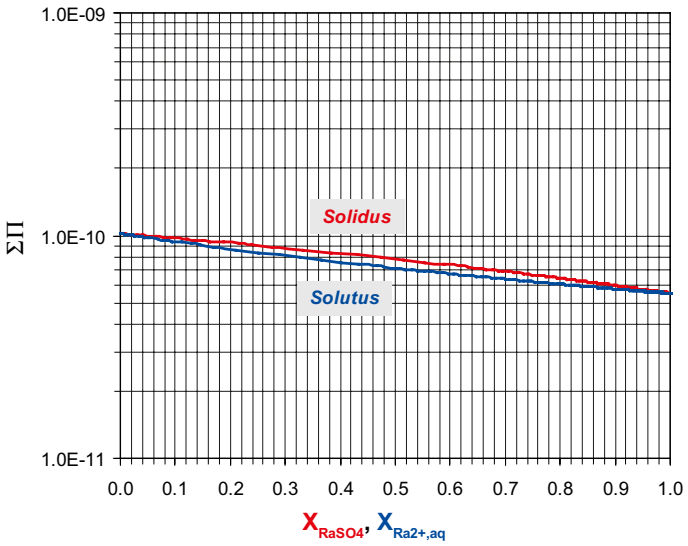

Figure A-1. *Lippmann diagram for the (Ba,Ra)SO_4 binary solid solution at 25°C. The SS system is assumed to be ideal (e.g. no dependence of solid activity coefficients on SS composition). Solidus and solutus curves are drawn. Log K_{sp} for end members are –10.26 ($RaSO_{4\,(c)}$) and –9.97 ($BaSO_4$), respectively.*

If the solid solution series is considered to be ideal, the distance between solidus and solutus curves depends on the difference in solubility products. This difference in the (Ba,Ra)SO_4 binary solid solution is very small (less than one logK_{sp} unit) and, consequently, both curves are close to each other (see Figure A-1). For a better explanation and visualization of the solid solution concepts, we use in this introduction the (Ba,Sr)SO_4 binary system, in which the solubility products of the end members are more contrasting ($10^{-6.63}$ vs. $10^{-9.97}$). The Lippmann diagram for this system is shown in Figure A-2. In this latter example, the diagram has been constructed considering a regular, non-ideal SS, with interaction parameters $a_0 = a_1 = 4.03$.

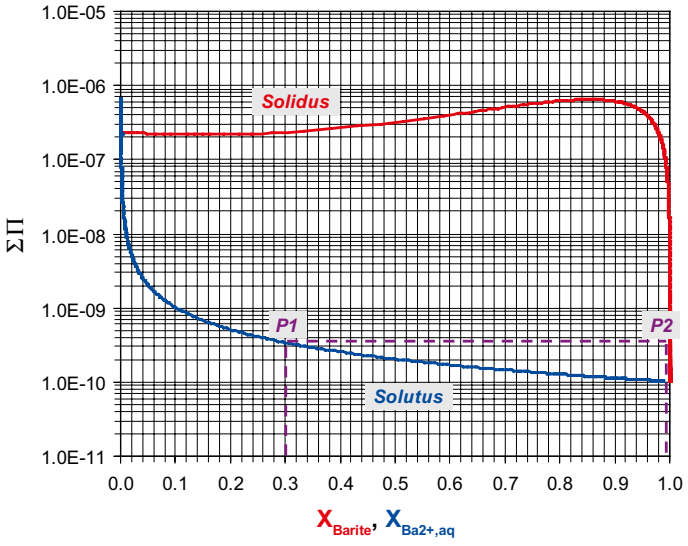

Figure A-2. *Lippmann diagram for the regular, non-ideal (Ba,Sr)SO_4 binary solid solution at 25°C. Solidus and solutus curves are drawn. Interaction parameters a_0 and a_1 are set to 4.03. P1 and P2 are tie lines that relate aqueous and SS compositions. Log K_{sp} for end members are –6.63 (celestite) and –9.97 (barite), respectively.*

In addition to Lippmann diagrams, SS system can also be represented in a partition diagram (also called *x-x* or Roozeboom diagrams). This plot allows the representation of aqueous activity mole fractions and the corresponding solid end-members mole fractions at equilibrium. This can help to visualize the affinity of an ion with respect to the solid phase. In the $(Ba,Sr)SO_4$ binary solid solution example, barium is strongly partitioned into the solid phase, as shown in Figure A-3); In contrast, strontium remains in solution. This extreme partition behaviour is mainly due to the large difference between solubility products of the end members.

As mentioned above, solubility products of the end members in the $(Ba,Ra)SO_4$ solid solution system are quite similar, implying a smaller partitioning of Ra into the solid phase (Figure A-4).

The distribution coefficient D, which depends on the solid composition in the case of non-ideal mixing, can be obtained from Equation A-10:

$$D = \frac{K_{RaSO_4} f_{RaSO_4}}{K_{BaSO_4} f_{BaSO_4}} = \frac{x_{BaSO_4} / x_{RaSO_4}}{[Ba^{2+}]/[Ra^{2+}]} \qquad \text{(Equation A-10)}$$

By combining Equations A-1, A-3, A-4 and A-10, we obtain the next expression (Equation A-11):

$$D = \frac{(x_{RaSO_4} - 1)x_{Ra^{2+},aq}}{x_{RaSO_4}(x_{Ra^{2+},aq} - 1)} \qquad \text{(Equation A-11)}$$

Equation A-11 allows the determination of activity coefficient or the solubility product of the solid solution end-member from a single experiment.

The main limitation of the Lippmann functions is found in the inability to deal with ternary (or higher order) solid solution systems, or aqueous equilibrium with two or more solid solutions /Kulik et al. 2000/.

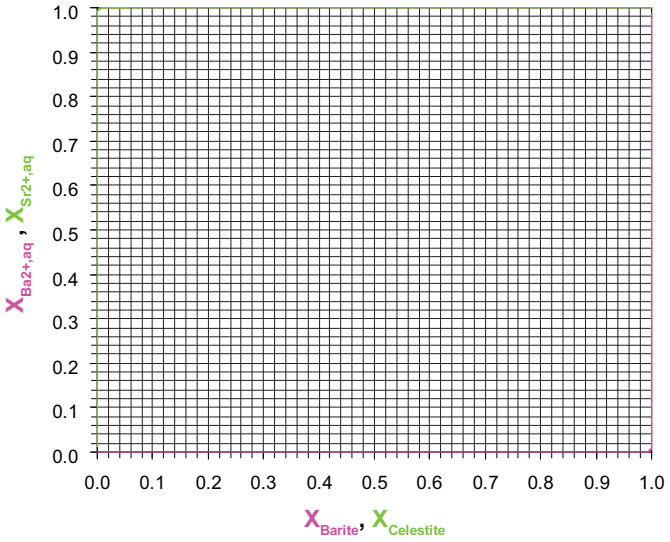

Figure A-3. *Partition diagram (or x-x, Roozeboom diagram) for the regular, non-ideal $(Ba,Sr)SO_4$ binary solid solution at 25°C. The curves are almost parallel with the ordinate and abscissa axis indicates strong partitioning of barium into the solid phase.*

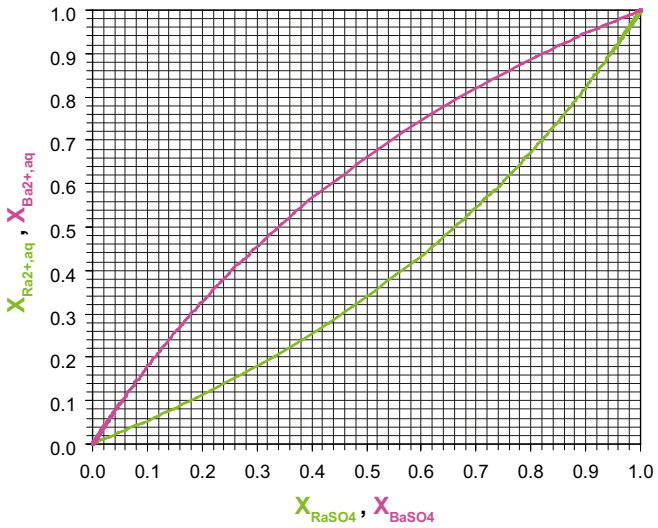

Figure A-4. *Partition diagram (or* ***x-x****, Roozeboom diagram) for the ideal (Ba,Ra)SO_4 binary solid solution at 25°C. Unlike the (Ba,Sr)SO_4 solid solution system, the similarity between solubility products of the end members lead to smaller partitioning of aqueous Ra into the solid phase.*

Appendix B

The Gibbs Energy Minimisation (GEM) approach and the GEMS-PSI code

The Gibbs Energy Minimisation approach (GEM) methodology is based on the concept introduced by Gibbs which states that the chemical potential of an element is the same in all co-existing phases at equilibrium /Kulik et al. 2004/. The equilibrium in the system is achieved when the total Gibbs free energy of this system is minimal at given conditions of T, P and composition.

Following the *unified theory of solid solution solubility* /Gamsjäger et al. 2000/, dissolution of a (Ba,Ra)SO_4 solid solution in aqueous medium can be written as Equation B-1:

$$nBa_{1-x_0}Ra_{x_0}SO_4(s) \rightarrow (n-\xi)Ba_{1-x}Ra_xSO_4(s) + \left[n(1-x_0) - (n-\xi)(1-x)\right]Ba^{2+}_{aq} + \left[nx_0 - (n-\xi)x\right]Ra^{2+}_{aq} + \xi SO_4{}^{2-}_{aq} \quad \text{(Equation B-1)}$$

where ξ is the reaction extent variable. The total Gibbs energy function G of this system is defined by Equation B-2:

$$G_{x,\xi} = (n-\xi)\left[(1-x)\mu^{(s)}_{BaSO_4} + x\mu^{(s)}_{RaSO_4}\right] + \left[n(1-x_0) - (n-\xi)(1-x)\right]\mu^{(aq)}_{Ba^{2+}} + \left[nx_0 - (n-\xi)x\right]\mu^{(aq)}_{Ra^{2+}} + \xi\mu^{(aq)}_{SO_4{}^{2-}} + n_w\mu_{H_2O} \quad \text{(Equation B-2)}$$

The general equilibrium condition is the minimum of total Gibbs energy function (Equation B-3)

$$dG = \left(\frac{\partial G}{\partial \xi}\right)_x d\xi + \left(\frac{\partial G}{\partial x}\right)_\xi dx = 0 \quad \text{(Equation B-3)}$$

where

$$\left(\frac{\partial G}{\partial \xi}\right)_x = \left[(1-x)\mu^{(aq)}_{Ba^{2+}} + x\mu^{(aq)}_{Ra^{2+}} + \mu^{(aq)}_{SO_4{}^{2-}}\right] - \left[(1-x)\mu^{(s)}_{BaSO_4} + x\mu^{(s)}_{RaSO_4}\right] \quad \text{(Equation B-4)}$$

$$\left(\frac{\partial G}{\partial x}\right)_\xi = (1-\xi)\left[\mu^{(s)}_{RaSO_4} - \mu^{(s)}_{BaSO_4} - \left(\mu^{(aq)}_{Ra^{2+}} - \mu^{(aq)}_{Ba^{2+}}\right)\right] \quad \text{(Equation B-5)}$$

Considering $\mu^{(aq)}_{BaSO_4} = \mu^{(aq)}_{Ba^{2+}} + \mu^{(aq)}_{SO_4{}^{2-}}$, $\mu^{(aq)}_{RaSO_4} = \mu^{(aq)}_{Ra^{2+}} + \mu^{(aq)}_{SO_4{}^{2-}}$ and $\Delta_{sol}\mu_{BaSO_4} = \mu^{(aq)}_{BaSO_4} - \mu^{(s)}_{BaSO_4}$, $\Delta_{sol}\mu_{RaSO_4} = \mu^{(aq)}_{RaSO_4} - \mu^{(s)}_{RaSO_4}$, then Equation B-3 can also be written as Equation B-6:

$$dG = \left[(1-x)\Delta_{sol}\mu_{BaSO_4} + x\Delta_{sol}\mu_{RaSO_4}\right]d\xi + \left[(1-\xi)\left(\Delta_{sol}\mu_{BaSO_4} - \Delta_{sol}\mu_{RaSO_4}\right)\right]dx = 0 \quad \text{(Equation B-6)}$$

From Equation B-3, equilibrium will be met when $\left(\frac{\partial G}{\partial \xi}\right)_x = 0$ and $\left(\frac{\partial G}{\partial x}\right)_\xi = 0$.

Following Equation B-6, this occurs if $\Delta_{sol}\mu_{BaSO_4} = 0$ (or $\mu^{(aq)}_{BaSO_4} = \mu^{(s)}_{BaSO_4}$) and $\Delta_{sol}\mu_{RaSO_4} = 0$ (or $\mu^{(aq)}_{RaSO_4} = \mu^{(s)}_{RaSO_4}$), i.e. when chemical potentials of all end-members are the same in the solid and the aqueous phase.

Thermodynamic partitioning can be obtained by considering $\left(\frac{\partial G}{\partial x}\right)_\xi = 0$; Thus,

$$\mu^{(s)}_{RaSO_4} - \mu^{(s)}_{BaSO_4} = \mu^{(aq)}_{Ra^{2+}} - \mu^{(aq)}_{Ba^{2+}} \quad \text{(Equation B-7)}$$

This expression, written in terms of molalities, can lead to a distribution coefficient:

$$D = \frac{x\,m_{Ba^{2+}}}{(1-x)m_{Ra^{2+}}} = \frac{K_{S,BaSO_4} f_{BaSO_4}\gamma_{Ra^{2+}}}{K_{S,RaSO_4} f_{RaSO_4}\gamma_{Ba^{2+}}} \quad \text{(Equation B-8)}$$

The solubility product of the binary mixture $Ba_{1-x}Ra_xSO_4$ can be defined as:

$$\left(a_{Ba^{2+}}^{(aq)} a_{SO_4^{2-}}^{(aq)}\right)^{1-x} \cdot \left(a_{Ra^{2+}}^{(aq)} a_{SO_4^{2-}}^{(aq)}\right)^{x} = \left(K_{S,BaSO_4} a_{BaSO_4}^{(s)}\right)^{1-x} \left(K_{S,RaSO_4} a_{RaSO_4}^{(s)}\right)^{x} = K_{S,BaRaSO_4}^{(x)} \qquad \text{(Equation B-9)}$$

Equation B-9 allows the linking between the activities of dissolved ions with that of solid mixture end members.

In the GEM approach, mass balance is made for the entire system. For the definition of the system, only the total amounts of the chemical elements involved (along with a charge balance) is required. These elements and the electric charge are called *independent components*, whereas chemical species are the *dependent components*. Activities and concentrations of the dependent components are treated separately for each phase, considering activity coefficients and standard states. A non-linear minimization algorithm iteratively finds the quantities of all relevant species that minimize the total Gibbs energy of the system. This method can solve complex SSAS equilibrium in one GEM run without any supporting tools such as Lippmann functions and semi-empirical iterative procedures required in SSAS speciation models based on the Law-of-Mass-Action. The applicability of GEM approach is only restricted by the availability of standard-state molar properties of end-members and the non-ideal interaction parameters for each phase.

One of the codes based on GEM formulation is GEMS-PSI /Kulik et al. 2004/. This code consists mainly of a non-linear minimisation algorithm, a thermodynamic database and a graphical user interface. Details of the internal calculation functions are reported in /Kulik et al. 2004/ and /Kulik 2006/.